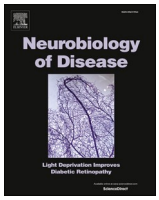
Neurobiology of Disease 152 (2021) 105278



Contents lists available at ScienceDirect

Neurobiology of Disease

journal homepage: www.elsevier.com/locate/ynbdi





Identification of the 5-HT$_{1A}$ serotonin receptor as a novel therapeutic target in a *C. elegans* model of Machado-Joseph disease

Joana Pereira-Sousa [a,b,c], Bruna Ferreira-Lomba [a,b], Aina Bellver-Sanchis [a,b,1], Daniela Vilasboas-Campos [a,b], Jorge H. Fernandes [a,b], Marta D. Costa [a,b], Mark A. Varney [d], Adrian Newman-Tancredi [d], Patrícia Maciel [a,b,*,2], Andreia Teixeira-Castro [a,b,*,2]

[a] Life and Health Sciences Research Institute (ICVS), School of Medicine, University of Minho, Braga, Portugal
[b] ICVS/3B's - PT Government Associate Laboratory Braga/Guimarães, Portugal
[c] Behavioral & Molecular Lab (Bn'ML), University of Minho, Braga, Portugal
[d] Neurolixis Inc., Park Ridge, NJ 07656, USA

ARTICLE INFO

Keywords:
Befiradol
NLX-112
5-HT$_{1A}$ receptor agonist
Spinocerebellar ataxia type 3
Ataxin-3 aggregation
Serotonin
Therapy

ABSTRACT

Machado-Joseph disease (MJD) or Spinocerebellar ataxia type 3 (SCA3) is a progressive neurodegenerative disorder that affects movement coordination leading to a premature death. Despite several efforts, no disease-modifying treatment is yet available for this disease. Previous studies pinpointed the modulation of serotonergic signaling, through pharmacological inhibition of the serotonin transporter SERT, as a promising therapeutic approach for MJD/SCA3. Here, we describe the 5-HT$_{1A}$ receptor as a novel therapeutic target in MJD, using a *C. elegans* model of ATXN3 proteotoxicity. Chronic and acute administration of befiradol (also known as NLX-112), a highly specific 5-HT$_{1A}$ agonist, rescued motor function and suppressed mutant ATXN3 aggregation. This action required the 5-HT$_{1A}$ receptor orthologue in the nematode, SER-4. Tandospirone, a clinically tested 5-HT$_{1A}$ receptor partial agonist, showed a limited impact on animals' motor dysfunction on acute administration and a broader receptor activation profile upon chronic treatment, its effect depending on 5-HT$_{1A}$ but also on the 5-HT$_6$/SER-5 and 5-HT$_7$/SER-7 receptors. Our results support high potency and specificity of befiradol for activation of 5-HT$_{1A}$/SER-4 receptors and highlight the contribution of the auto- and hetero-receptor function to the therapeutic outcome in this MJD model. Our study deepens the understanding of serotonergic signaling modulation in the suppression of ATXN3 proteotoxicity and suggests that a potent and selective 5-HT$_{1A}$ receptor agonist such as befiradol could constitute a promising therapeutic agent for MJD.

1. Introduction

Machado-Joseph disease (MJD) or Spinocerebellar ataxia type 3 (SCA3) is a dominantly inherited neurodegenerative disease caused by an abnormal expansion of the cytosine-adenosine-guanine triplet (CAG) that encodes the amino acid glutamine in the ataxin-3 protein (ATXN3). Although the genetic alteration that causes MJD was described more than 25 years ago (Kawaguchi et al., 1994), currently, there is no treatment available for this severe and ultimately fatal disorder. MJD is the most prevalent form of dominant cerebellar ataxia worldwide and its clinical symptoms include progressive cerebellar ataxia, pyramidal syndrome, peripheral neuropathy, oculomotor abnormalities, extrapyramidal signs and sleep perturbation (Mendonca et al., 2018). At the molecular level, the abnormal expansion of the CAG repeat in the ataxin-3 gene translates into a polyglutamine tract of 61 to 87 glutamines that renders ATXN3 prone to self-assembly, and thus to form aggregates, and makes it toxic to neurons. The pathophysiology of MJD has been widely studied in the last decades, pointing to the misfolding of mutant ATXN3 and the disruption of protein homeostasis as the hub of MJD pathogenesis (reviewed in (Da Silva et al., 2019)).

In an attempt to counteract MJD progression, several studies were carried out using targeted- or hypothesis-free strategies to find disease-

* Corresponding authors at: Life and Health Sciences Research Institute (ICVS), School of Medicine, University of Minho, Braga, Portugal.
E-mail addresses: pmaciel@med.uminho.pt (P. Maciel), accastro@med.uminho.pt (A. Teixeira-Castro).
[1] Current affiliation: Pharmacology Section, Department of Pharmacology, Toxicology and Therapeutic Chemistry, Faculty of Pharmacy and Food Sciences, Institut de Neurociències—Universitat de Barcelona, Avda. Joan XXIII, 27. 08028 Barcelona, Spain.
[2] Authors share senior authorship.

https://doi.org/10.1016/j.nbd.2021.105278
Received 27 October 2020; Received in revised form 15 January 2021; Accepted 24 January 2021
Available online 28 January 2021
0969-9961/© 2021 The Authors. Published by Elsevier Inc. This is an open access article under the CC BY-NC-ND license (http://creativecommons.org/licenses/by-nc-nd/4.0/).

modifying compounds capable of ameliorating core symptoms of the disease (Da Silva et al., 2019; Neves-Carvalho et al., 2020). Some of the compounds described in these studies are neuromodulators including compounds that target the neuropeptide Y, and the adenosinergic, dopaminergic or serotonergic systems (Costa et al., 2016; Duarte-Neves et al., 2015; Goncalves et al., 2017; Teixeira-Castro et al., 2015). Previously, in an unbiased in vivo screening, we found that treatment with citalopram, a selective serotonin reuptake inhibitor (SSRI) that targets the serotonin transporter (SERT), suppressed mutant ATXN3 proteotoxicity in *C. elegans* and in two distinct transgenic mouse models of MJD (Ashraf et al., 2019; Esteves et al., 2019; Teixeira-Castro et al., 2015). Consistently with the pharmacological effect of citalopram, the molecular ablation of the *C. elegans* SERT homologue, MOD-5, suppressed mutant ATXN3 aggregation and motor impairments. Treatment efficacy was dependent on SERT/MOD-5 but also on serotonin (5-HT) receptors, their direct targeting, using pharmacological modulators, being sufficient to significantly reduce the motor dysfunction of the nematode MJD model (Teixeira-Castro et al., 2015).

Although citalopram and other SSRIs directly bind and inhibit SERT, thereby increasing the 5-HT availability at the synapse, there is, at least in the context of depression treatment, a delay in time to first response (Schatzberg, 2002). This is likely due to the molecular dynamics of 5-HT_{1A} receptors (5-HT_{1A}Rs). 5-HT_{1A}R is one of the most abundant and widely expressed 5-HT receptors in the brain (Albert et al., 1990; Garcia-Garcia et al., 2014; Pompeiano et al., 1992). There are two distinct populations of 5-HT_{1A}Rs: the presynaptic autoreceptors located on the cell body and dendrites of 5-HT neurons of the dorsal raphe nuclei (DRN); and the postsynaptic somatodendritic heteroreceptors expressed at 5-HT projecting areas (Kia et al., 1996; Riad et al., 2000). 5-HT_{1A} autoreceptors negatively regulate the 5-HT system. Serotonin released from the DRN activates 5-HT_{1A} autoreceptors, which exert a feedback inhibition on the firing of 5-HT neurons (Albert and Vahid-Ansari, 2019; Invernizzi et al., 1988; Prinssen et al., 2002; Stahl, 1998). In addition to their direct effect at the serotonin transporter, the chronic administration of SSRIs is accompanied by the downregulation of the 5-HT_{1A} autoreceptors and the subsequent suppression of the negative feedback mechanism of the serotonergic system, increasing neuronal firing rate (Kulikov et al., 2018; Stahl, 1998). Release of serotonin in target brain regions, in contrast, activates 5-HT heteroreceptors, including the 5-HT_{1A} heteroreceptor, which are associated to multiple regulatory functions including neuronal plasticity and synaptogenesis (Albert and Vahid-Ansari, 2019). Moreover, 5-HT_{1A}R can play a role in motor fine tuning and coordination, and it has been shown that several 5-HT_{1A}R agonists exhibited pronounced neuroprotective properties in models of cell injury, by causing a reduction in glutamate release and through the regulation of anti-apoptotic activities and the expression of protective proteins (Berends et al., 2005; Druse et al., 2005; Miyazaki and Asanuma, 2016; Oosterink et al., 2003; Thampi et al., 2012).

Tandospirone, a partial 5-HT_{1A}R agonist, has been used in the clinic to treat anxiety and depression and was put forward as a candidate for the treatment of other central nervous system disorders, including Parkinson, Alzheimer's and schizophrenia (Huang et al., 2017). Furthermore, treatment with tandospirone reduced ataxia, pain, insomnia and depressive symptoms in spinocerebellar ataxia (SCA) patients (Takei et al., 2003; Takei et al., 2010; Takei et al., 2005), focusing attention on the 5-HT_{1A} receptor as a promising target for the treatment of SCAs, including MJD.

Befiradol (NLX-112, F-13640) is a selective, full agonist that displays high selectivity and maximum potency at 5-HT_{1A}R (Colpaert et al., 2002; Newman-Tancredi et al., 2017), binding preferentially to subcortical regions of the brain in several species including non-human primates (Vidal et al., 2018). Other animal studies showed therapeutic efficacy in a range of models of movement disorders, including efficacious anti-dystonic activity in rat, namely by eliminating the catalepsy induced by the neuroleptic drug, haloperidol, and the complete reversal of L-DOPA-induced dyskinesia in parkinsonian rats (Iderberg et al., 2015). These effects appear to translate well to higher species, because befiradol also elicits potent and efficacious anti-dyskinetic and anti-parkinsonian-like properties in MPTP-treated marmosets and MPTP-treated macaques (Depoortere et al., 2020; Fisher et al., 2020). Furthermore, previous clinical trials of befiradol indicate that it is well-tolerated and safe (EU_Clinical_Trials, 2009; Paillard et al., 2020), suggesting that it has potential for treating CNS disorders involving serotonergic transmission.

Here, we take advantage of the *C. elegans* model of ATXN3-proteotoxicity (ATXN3 mutant), to test the effect of befiradol in motor dysfunction and aggregation, not only under chronic treatment but also upon acute administration of the drug. In this animal model, a mutant form of human ATXN3 with 130 glutamines, expressed in *C. elegans* neurons, leads to protein aggregation and motor dysfunction phenotypes, which, as in humans, is highly dependent on the size of the polyQ expansion and progresses with aging (Teixeira-Castro et al., 2011a). Despite its simplicity and relatively small number of neurons, the short life cycle, the conservation of basic cellular mechanisms and the phenotypic similarities with human MJD pathogenesis, conjugated with the possibility of genetic manipulation, make *C. elegans* a potent platform for drug testing and target validation *in vivo*. In addition to the therapeutic effect of befiradol treatment, we show high selectivity of this drug for the 5-HT_{1A}R orthologue SER-4 in *C. elegans*, in comparison with tandospirone that shows limited effect under acute treatment and an additional requirement for the presence of the 5-HT_6 and 5-HT_7 (SER-5 and SER-7, respectively) receptors activity at chronic administration. The finding that befiradol is a potent and selective disease-modifying compound for MJD may be relevant for future treatment of this and other disorders of protein conformation.

2. Materials & methods

2.1. Nematode strains and general methods

Strains used in this work and abbreviations are listed in Supplementary Table 1. All the strains were backcrossed to Bristol strain N2 (WT) five to twelve times. Standard methods were used for culturing and observing *C. elegans*, unless otherwise noted (Brenner, 1974). Nematodes were grown on nematode growth medium (NGM) plates seeded with Escherichia coli OP50 strain at 20 °C.

2.2. Drug assay

The drug assay was performed in a 96-well plate format, in liquid culture (Voisine et al., 2007). Each well contained a final volume of 60 µl, comprising 20–25 animals for wild-type (WT, N_2) and wild-type ATXN3 (ATXN3 WT), or 40–45 animals for mutant ATXN3 (ATXN3 mutant or AT3q130) in egg stage in 15 µl, 25 µl of drug at the appropriate concentration and 20 µl of OP50 bacteria to a final optical density at 595 nm (OD_{595}) of 0·9 measured in the microplate reader (Tecan Infinite 200 Microplate Reader).

To obtain an age synchronized population of eggs, four-day-old gravid adults were treated with alkaline hypochlorite solution (0·5 M NaOH, ~2·6% NaClO) for five minutes. The animals were then washed in M9 buffer, resuspended in S-medium (S-Basal, 10 mM potassium citrate pH 6, 10× trace metals solution, 3 mM $CaCl_2$, 3 mM $MgSO_4$) to the appropriate egg number and transferred into the 96-well plate. The OP50 bacteria were grown overnight at 37 °C and 150 rpm in Luria Broth (LB) media, pelleted by centrifugation, inactivated by three cycles of freeze/thawing, frozen at −80 °C and then resuspended in S-medium supplemented with 0·004 mg/ml cholesterol, 0·5× Pen-strep (Sigma) and 0·5× nystatin (Sigma). Worms were grown with continuous shaking at 180 rpm at 20 °C (Shel Lab) for four days.

2.3. Compound preparation

Compounds used in this study were provided by Neurolixis or were obtained from the commercial vendors indicated below and were used without further purification. To define the optimal concentration of the compounds, befiradol (a.k.a. NLX-112 or F13640; Neurolixis, CAS# 208110–64-9) and tandospirone (Aris Pharmaceuticals or Chemvon Industries CAS# 112457–95-1) were serially diluted in a range between 50 mM and 0·00001 mM in 100% dimethyl sulphoxide (DMSO, Sigma). Each concentration was then diluted in MiliQ purified water to obtain, in the well, a final concentration ranged between 500 μM and 0·01 nM in 1% DMSO. Further assays, with chronic or acute treatment protocols, were performed using 10 μM concentration of befiradol or tandospirone. Estrone (Sigma, CAS# 53-16-7) was diluted to a 25 μM concentration, WAY-100635 maleate (Tocris Bioscience, CAS# 1092679-51-0) was diluted to a 0·1 μM, 1 μM and 10 μM concentrations. 17-DMAG (Tocris Bioscience, CAS# 467214-21-7) was diluted to 1 μM concentration in water and CCI779 (LC Laboratories, CAS# 162635-04-3) was diluted to 1 μM concentration in 0·02% ethanol.

2.4. Food clearance assay

WT worms were subjected to a drug assay as described above, except for the OP50 bacteria OD_{595} adjusted to 0·7 (Voisine et al., 2007). Worms were grown with continuous shaking at 180 rpm at 20 °C (Shel Lab) for seven days. Befiradol and tandospirone stock concentrations were prepared in 100% DMSO (Sigma) and tested at dilutions corresponding to a maximum concentration of 1% DMSO to avoid solvent-specific developmental defects and toxicity. Tested concentrations ranged between 500 μM and 0·01 nM. The effect of compounds on *C. elegans* physiology was monitored by the rate at which the OP50 suspension was consumed, as a read out for *C. elegans* growth, survival, or fecundity. The OD_{595} was measured daily. OP50-only (S-medium, no vehicle), DMSO 1% (vehicle) and DMSO 5% (toxic condition) controls were used.

2.5. C. elegans assays

2.5.1. Motility assay and motor index determination

Four-day-old animals were transferred from the 96-well plates onto an unseeded NGM plate (equilibrated at 20 °C). Plates were allowed to dry for 45 min before starting the motility assays. Motility assays were performed at 20 °C as previously described (Teixeira-Castro et al., 2011a). Five animals were placed simultaneously in the center of a freshly seeded 30 mm plate, equilibrated at 20 °C. Animals remaining inside the 1 cm circle after one minute were scored as locomotion-defective. Motor behavior assays were run in triplicates or quadruplicates (n = 3 or 4), with a total of at least 150 animals tested per compound concentration.

Motor index establishes a score, in which treated animals that display the same motor behavior as mutant ATXN3 had a 0% index and when animals improve motor coordination comparable with ATXN3 WT expressing animals obtain an index of 100%. All results shown in the figures are calculated using the following formula

$$\text{Motor index } (\%) = \frac{\text{LD mutant ATXN3}_{\text{vehicle}} - \text{LD mutant ATXN3}_{\text{drug}}}{\text{LD mutant ATXN3}_{\text{vehicle}} - \text{LD ATXN3 WT}_{\text{vehicle}}}$$

LD- locomotion-defective.

2.5.2. Velocity assay

Wild-type (WT), wild-type ATXN3 (ATXN3 WT) and mutant ATXN3 (ATXN3 mutant or AT3q130) animals were grown in liquid culture in a 96-well plate format as described above. Four-day-old animals grown in vehicle (1% DMSO) or treated chronically with 10 μM befiradol or 10 μM tandospirone were transferred to climatized NGM plates without OP50 and after 45 min velocity assays were performed. For the velocity assay set up, the recording system comprised a stereo microscope (SZX7, Olympus), a digital camera (SC30, Olympus) and an imaging software (Olympus cellSens Software, RRID:SCR_016238) and 30 mm seeded NGM plates with a cooper ring in the center (assay plate) were used to avoid the escape of worms from the camera field. The assay was performed at 20 °C. Ten to 15 animals were transferred to the middle of the assay plate and movements were recorded immediately. A 0·8 X zoom lens was used to maximize the recorded field. Animals were recorded during 1 min at a rate of 15 frames per second. Recorded images were analysed by ImageJ (ImageJ, RRID:SCR_003070) and wrMTrck (plugin for ImageJ: www.phage.dk/plugins). The locomotion velocity was obtained in μm per second and corrected for the size of the animal (Body Length per second (BLPS) data in wrMTrck) (Nussbaum-Krammer et al., 2015). Animals that were recorded for less than 25 s were discarded.

2.5.3. C. elegans assays for aggregation

For confocal dynamic imaging and quantification of ATXN3 aggregation, mutant ATXN3 animals were grown in liquid culture in a 96-well plate format, with 10 μM befiradol or 10 μM tandospirone, as described above. For this assay, drugs were added at egg stage (chronic treatment) or 2 h before the acquisition (acute treatment). Four-day-old animals were transferred from the 96-well plates onto unseeded NGM plates (equilibrated at 20 °C). After 45 min, live animals were immobilized with 3 mM levamisole (Sigma) and mounted on a 3% agarose pad. All images were captured using an Olympus LPS Confocal FV1000 microscope (Confocal microscope, Olympus, FV1000, RRID:SCR_016840) under a 60× oil (NA = 1·35) objective. *Z*-series imaging was acquired for all vehicle- and befiradol-treated and tandospirone-treated animals, using a 515 nm laser excitation line for yellow fluorescent protein fusion proteins. The pinhole was adjusted to 1·0 Airy unit of optical slice, and a scan was acquired every ~0·5 μm along the *z*-axis. The quantification of the aggregates was performed as previously described (Teixeira-Castro et al., 2011a; Teixeira-Castro et al., 2011b). Three parameters were extracted from analysis: area of aggregates/total area; number of aggregates/total area and total area. Values shown are the mean (normalized to vehicle treated control) of nine or more animals per group, unless otherwise noted.

For filter trap assay and biochemical fractionation, worms were grown in liquid culture in a 96-well plate format, treated chronically or acutely with 10 μM befiradol, as described before. A total of 1500 eggs were plated for WT, ATXN3 WT and *mod-5*Δ; AT3q130 strains and 2500 eggs were plated for mutant ATXN3 vehicle-treated and befiradol-treated conditions. Four-day-old animals were collected and washed three times with M9, to eliminate OP50 bacteria and progeny, and flash-frozen in liquid nitrogen. For protein/aggregates extraction, a 50 μl of non-denaturating protein buffer (50 mM HEPES, pH 7·4, 150 mM NaCl, 1 mM EDTA, 0·5% Triton X-100) or 150 μl of RIPA buffer (50 mM Tris, pH 7·5, 150 mM NaCl, 25 mM EDTA, 0·2% Triton X-100), for filter trap or biochemical fractionation respectively, freshly supplemented with EDTA-free protease inhibitor cocktail (Roche) was added and worms were disrupted by mechanic force using glass beads (Sigma) in a FastPrep®-24 (MP Biomedicals) (six cycles of 6·5 ms for 45 s followed by 1 min on ice). After a centrifugation of 500 *g* during 1 min, the supernatant was collected, and the total protein quantified by the Bradford assay (Bio-Rad). For filter trap, a total of 100 μg of protein was treated with SDS at a final concentration of 1% and loaded onto a cellulose acetate membrane assembled in a slot blot apparatus (Bio-Rad). The membrane was washed with 0·1% SDS and retained ATXN3 protein detected with anti-ATXN3 mouse (1:1000) (Millipore Cat# MAB5360, RRID: AB_2129339) and with horseradish peroxidase-coupled secondary antibodies (Bio-Rad) and chemiluminescence (ECL Radiance, Azure Biosystems). For biochemical fractionation, protein concentration was adjusted to 4 μg/μl and followed by a 22,000 *g* centrifugation for 30 min at 4 °C. The pellet fractions were separated from supernatants (Triton X-100-soluble fraction) and homogenized in 150 μl RIPA buffer

supplemented with 2% SDS, followed by a second centrifugation step at room temperature. The supernatants (SDS-soluble fraction) were removed, and the remaining pellets were incubated for 16 h in 100% formic acid at 37 °C allowing formic acid evaporation. Pellet was dissolved in 50 µl of Laemmli buffer (0·1 M Tris (pH = 6·8), 16% glycerol, 2% SDS, β-mercaptoethanol and bromophenol blue powder) (SDS-insoluble fraction). For SDS–polyacrylamide gel electrophoresis 50 µg of the Triton X-100 fraction, 40 µl of the SDS-soluble fraction and the complete SDS-insoluble fraction were loaded in a 10% SDS gel. ATXN3 protein was detected with anti-ATXN3 mouse (1:1000) (Millipore Cat# MAB5360, RRID: AB_2129339) and with horseradish peroxidase-coupled secondary antibodies (Bio-Rad) and chemiluminescence (ECL western-blotting detecting reagents, Bio-Rad or ECL Radiance, Azure Biosystems). The capture of chemiluminescence signals was performed in the Sapphire Biomolecular Imager (Azure Biosystems), and Western blot quantifications were performed using AzureSpot Analysis Software (Azure Biosystems), according to the manufacturer's instructions.

2.5.4. *C. elegans* ratiometric calcium dynamic imaging

Ratiometric calcium imaging was performed as previously described (Collins et al., 2016; Ravi et al., 2018b). Briefly, for ratiometric Ca^{2+} dynamic imaging and quantification in the HSN neuron, *nlp-3*::GcAMP5 animals were grown in liquid culture in a 96-well plate format, with 10 µM befiradol as described above. Drugs were added at the egg stage (chronic treatment) or 2 h before image acquisition (acute treatment). Four-day-old animals were immobilized with 5 mM levamisole (Sigma) and mounted on a 3% agarose pad. After 30 min, images were captured using a Confocal Laser Scanning Microscope FV3000 (Olympus Confocal Laser Scanning Microscope Fluoview FV3000, RRID:SCR_017015) with the resonant scanner running at 8000 Hz and collected at 30 fps at 512 × 512 pixel resolution, 16-bit depth after 2× digital zoom, under a 60× oil (NA = 1·35) objective. Time-series images were acquired for all vehicle- and befiradol-treated animals at each 30 ms during 15 min, using a 488 nm laser excitation line for GcAMP5, and 651 nm laser excitation line for mCherry. Both proteins expressed, under the same promoter (*nlp-3*), in the HSN neuron. Acquisition of each channel was done simultaneously. The pinhole was adjusted to 1·15 Airy unit of optical slice. The quantification of fluorescence intensity for both channels was performed using Fiji ImageJ software (Fiji, RRID: SCR_002285). After subtraction of background intensity, R and ΔR/R values were calculated using the following formulas:

$$R = \frac{F_{GcAMP5}}{F_{mCherry}} \quad \Delta R/R = \frac{R_{t(x)} - R_{t(lowestR)}}{R_{t(lowestR)}}$$

2.6. SDS-PAGE and Western blot

For determination of the steady-state protein levels of ATXN3, mutant ATXN3 animals were incubated in liquid culture with vehicle (1% DMSO), 10 µM befiradol or 10 µM tandospirone in a 96-well plate format as already mentioned. For chronic treatment, four-day-old animals were transferred from the liquid culture onto an unseeded NGM plate (equilibrated at 20 °C). After 45 min, 25 individual young adult animals were picked into a screwed Eppendorf tube, boiled for 15 min in sodium dodecyl sulphate (SDS) sample buffer (to destroy all the aggregates) and the resulting extracts resolved on a 10% SDS gel, as previously described (Gidalevitz et al., 2009; Teixeira-Castro et al., 2011a). Immunoblots were probed with anti-ATXN3 mouse (1:1000) (Millipore Cat# MAB5360, RRID: AB_2129339) and anti-tubulin mouse antibodies (1:3000) (Sigma-Aldrich Cat# T5168, RRID: AB_477579); and detected with horseradish peroxidase-coupled secondary antibodies (Bio-Rad) and chemiluminescence (ECL Western-blotting detecting reagents, Bio-Rad). To capture chemiluminescence signal were used Chemidoc XRS Software (Bio-Rad) and Western blot quantifications were performed using ImageLab Software (Bio-Rad, RRID: SCR_014210), according to the manufacturer's instructions. For acute treatment, four-day-old animals treated with befiradol or tandospirone during 2 h in adulthood, were collected and washed three times with M9, and flash-frozen in Liquid Nitrogen. After extraction with 50 µl of non-denaturating protein buffer (50 mM HEPES, pH 7·4, 150 mM NaCl, 1 mM EDTA, 0·5% Triton X-100) freshly supplemented with EDTA-free protease inhibitor cocktail (Roche), worms were disrupted by mechanic force using glass beads (Sigma) in a FastPrep®-24 (MP Biomedicals) (six cycles of 6·5 ms for 45 s followed by 1 min on ice). After a centrifugation of 500 *g* during 1 min, the supernatant was collected, and the total protein quantified by the Bradford assay (Bio-Rad). 5 µg of total protein were transferred to an Eppendorf screw tube, supplemented with Laemmli Buffer to final 1× concentration and boiled for 15 min. The samples were resolved in a 10% SDS-gel, as previously described (Gidalevitz et al., 2009; Teixeira-Castro et al., 2011a). After transfer, membrane was incubated with AzureRed Fluorescent Total Protein Stain (Azure Biosystems) as manufacturer instructions. Immunoblots were probed with anti-ATXN3 mouse (1:1000) (Millipore Cat# MAB5360, RRID: AB_2129339) and detected with horseradish peroxidase-coupled secondary antibodies (Bio-Rad) and chemiluminescence (Radiance ECL, Azure Biosystems). To capture chemiluminescence signal were used Sapphire Biomolecular Imager (Azure Biosystems) and Western blot quantifications were performed using AzureSpot Analysis Software (Azure Biosystems), according to the manufacturer's instructions.

2.7. Generation of *C. elegans* double mutant strains

Males of *ser-5*Δ (tm2654), *ser-7*Δ (DA2100), mod-*1*Δ (MT9668), *dop-1*Δ (LX636) and *dop-2*Δ (LX702) were generated by mating with N2 (WT) males. To generate double mutant strains, thirteen males and three hermaphrodites L4 stage of ATXN3 mutant (AT3q130) (MAC001/AM685) animals were placed in NGM 30 mm seeded plate at 16 °C for 24 h. Hermaphrodites were singled out and male progeny were evaluated three days later. 24 to 32 L4 stage animals, from plates with 50% male progeny, were singled out and after 24 h worm lysis and single-worm PCR was performed to evaluate animals' genotype.

To generate double mutant strain lacking *tph-1* gene into ATXN3 mutant background, CRISPR/Cas9 technology was used as previously described (Paix et al., 2015). To generate *tph-1*Δ(mnh5) CRISPR RNAs (crRNAs) were designed using the Custom Alt-R® CRISPR-Cas9 guide RNA tool (Integrated DNA Technologies, Coralville, IA) and crRNAs with high on-target efficiency and low off-target prediction scores were chosen. To delete the complete gene sequence without altering regulatory regions, two crRNAs were designed, one to cut the 5′ region close to ATG start codon (cattgctctcttcaatcata) and another for the 3′ region near the stop codon triplet (ctacatcctgtagtttgagt). A single-stranded oligodeoxynucleotide (ssODN) comprising a fusion of the 5′ and 3′ regions flanking ATG and STOP codon triplet, respectively, (ctttggtttttaggtagcattgctctcttcaatcattttgagtttccgtgtttttttatttttttttatttgg) was used as a repair template. crRNA and ssODN repair template for *dpy-10* was co-injected with *tph-1* specific oligos and was used as a marker for efficiency of Cas9 activity. The injection mix, constituted by crRNAs, ssODNs and EnGen® Cas9 NLS, S. pyogenes enzyme (New England BioLabs, Ipswich, MA), was placed at 37 °C for 15 min, and young adult ATXN3 mutant (AT3q130) animals were injected, as previously described (Mello et al., 1991). Injected animals were placed at 25 °C and their progeny was screened for the roller phenotype 72 h later. Non-roller animals were singled out to avoid *dpy-10* mutation and screened by PCR for the *tph-1* deletion.

To lysate, each animal was placed in 10 µl of worm lysis buffer (50 mM KCl, 10 mM Tris-HCl (pH 8·3), 2·5 mM $MgCl_2$, 0·45% Nonidet P-40, 0·45% Tween 20, 0·01% (*w/v*) gelatin) supplemented with 0·01 µl of 20 mg/ml Proteinase-K and heated at 65 °C during 1 h. After Proteinase-k inactivation (95 °C, 15 min), 2 µl of worm lysate were used as template for Polymerase Chain Reaction (PCR) [1× Supreme NZYTaq II Green Master Mix, 200 nM primers (Supplementary table 2)]. PCR products were analysed in 1·5% agarose gel. 24 to 32 adult worms from

heterozygous plates were singled out and after genotype confirmation, by single worm PCR, and YFP fluorescence screening to confirm ATXN3 mutant (AT3q130) homozygosity in progeny, the double mutant strains and the ATXN3 mutant (AT3q130) post-crossing control were isolated.

For CRISPR/Cas9 *tph-1*Δ double mutant deletion was confirmed by Sanger sequencing.

2.8. Reverse-transcriptase quantitative PCR

Worm pellets from four-day-old animals were obtained by bleaching synchronization and washed four times with M9, resuspended in TRIzol™ (Invitrogen) and stored after flash freezing in liquid nitrogen. After thawing, worms were disrupted by mechanic force using glass beads (Sigma) in a FastPrep®-24 (MP Biomedicals) (six cycles of 4 ms for 30 s followed by one minute on ice). Beads were removed from the homogenate and a phase separation was conducted using chloroform retrieving the aqueous phase. RNA was extracted using RNeasy plus mini kit (Qiagen) according to the manufacturer's instructions. Samples were treated with DNase I (Thermo Scientific), RNA concentration was quantified by spectrophotometry, and RNA quality was tested through electrophoresis. cDNA was synthesized from 1 μg purified RNA using the iScript™ cDNA synthesis kit (Bio-Rad). The quantitative PCR was then carried out using the 5× HOT FIREPol® EvaGreen® qPCR Mix Plus (ROX) (Solis BioDyne) with 1 μl of cDNA. The used primers are listed in supplementary table 3. PCR reaction was run in Applied Biosystems™ 7500 Real-Time PCR System (Applied Biosystems) and raw data was extracted using 7500 software v2·3 (7500 Real-Time PCR Software, RRID:SCR_014596). Statistical analysis was conducted using $2^{-\Delta CT}$ values and plots was reported in Fold Change ($2^{-\Delta\Delta CT}$) (Livak and Schmittgen, 2001).

2.12. Statistical analysis

All statistical analysis was performed using the IBM SPSS statistics 23 software (SPSS, RRID:SCR_002865) and GraphPad Prism 8·0·1 software. Normal distribution of continuous variables was analysed according with Shapiro-Wilk or Kolmogorov-Smirnov normality test, depending on sample size, and histogram plot distribution. Levene's test assessment was performed to confirm homogeneity of variances between groups. When both assumptions were verified, groups were compared using independent sample *t*-test (Fig. 2b, c and d – befiradol chronic), one-way or two-way ANOVA followed by Dunnett (Fig. 1a – befiradol; Fig. 1b; Fig. 1d; Fig. 2d – acute and tandospirone chronic; Fig. 2g; Fig. 2h; Supplementary Fig. 2d), Tukey (Fig. 1b; Fig. 3; Supplementary Fig. 2a and b; Supplementary Fig. 4c and 2e) or Sidak post-hoc tests (Fig. 1c; Fig. 1d; Fig. 5b; Supplementary Fig. 4d; Supplementary Fig. 5). For Biochemical fractionation one-sample t-test with Bonferroni correction *versus* the value of 1 was applied (Fig. 2e and f).

When previous assumptions were not verified, a robust ANOVA (using R batch for SPSS) with Brown-Forsythe (if sample size less than 6) or Welch correction was reported and bootstrap with BCA were performed. Bootstrap sampling was followed by one-way ANOVA with

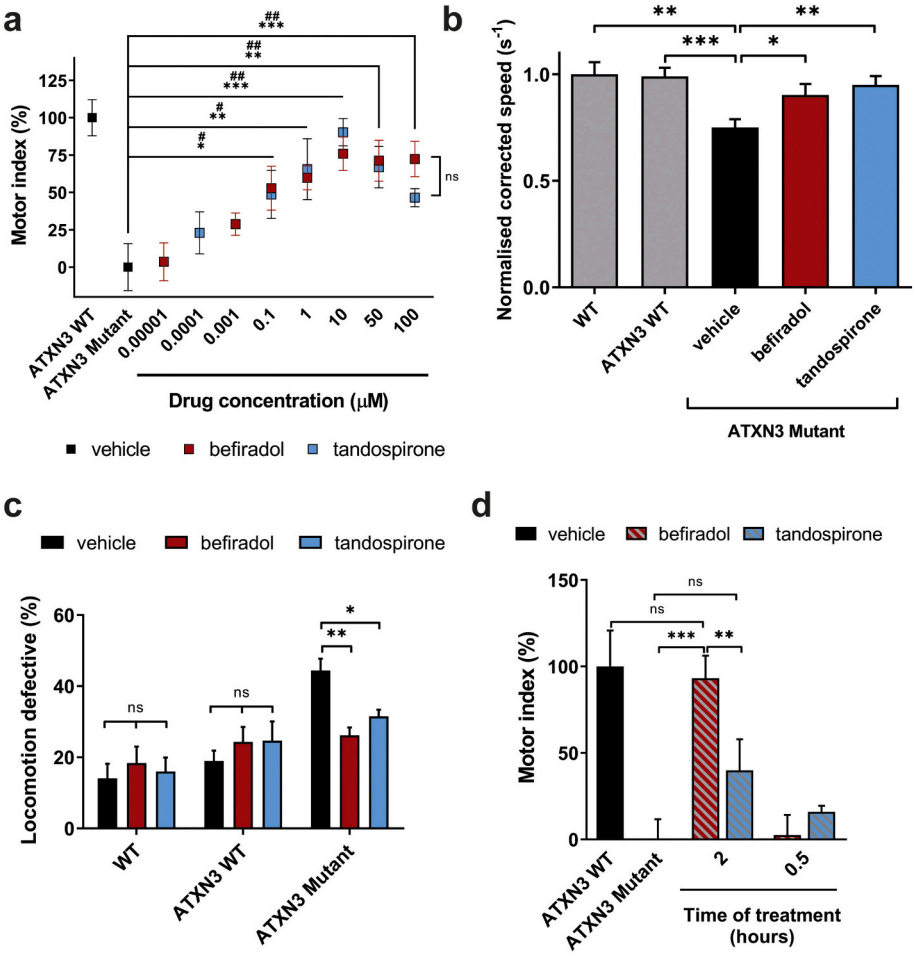


Fig. 1. Treatment with befiradol ameliorates motor dysfunction of ATXN3 mutant (AT3q130) animals. (a) befiradol (red) and tandospirone (blue) showed a positive impact on animals' motor dysfunction in the range of concentrations from 100 nM to 100 μM, the maximum effect being obtained at a 10 μM concentration for both drugs. (b) AT3q130 (ATXN3 mutant) animals presented a decreased corrected speed when compared to WT and ATXN3 WT animals. After chronic treatment with befiradol or tandospirone there was an increase in animals' velocity. (c) Chronic treatment with befiradol or with tandospirone did not change motor behavior of WT and ATNX3 WT animals. (d) Treatment of AT3q130 (ATXN3 mutant) animals during 2 h with befiradol ameliorates motor dysfunction. For dose-response (a): befiradol - (n = 7, ± SEM) *P < 0·05, **P < 0·01, ***P < 0·001 (ANOVA, Dunnett test); tandospirone – (n = 6, ± SEM) $^{\#}$P < 0·05, $^{\#\#}$P < 0·01 (ANOVA, SIDAK test corrected for BCA). Velocity assay (b): (n = 18–43, ± SEM), *P < 0·05, **P < 0·01, ***P < 0·001 (ANOVA, Dunnett test). Drug effects on wild-type animals (c): (n = 4, ± SEM) *P < 0·05, **P < 0·01, ns – non-significant (ANOVA, SIDAK test). Acute treatment assay (d): (n = 3, ± SEM) **P < 0·01, ***P < 0·001, ns – non-significant (Factorial ANOVA, SIDAK test and Dunnett test).

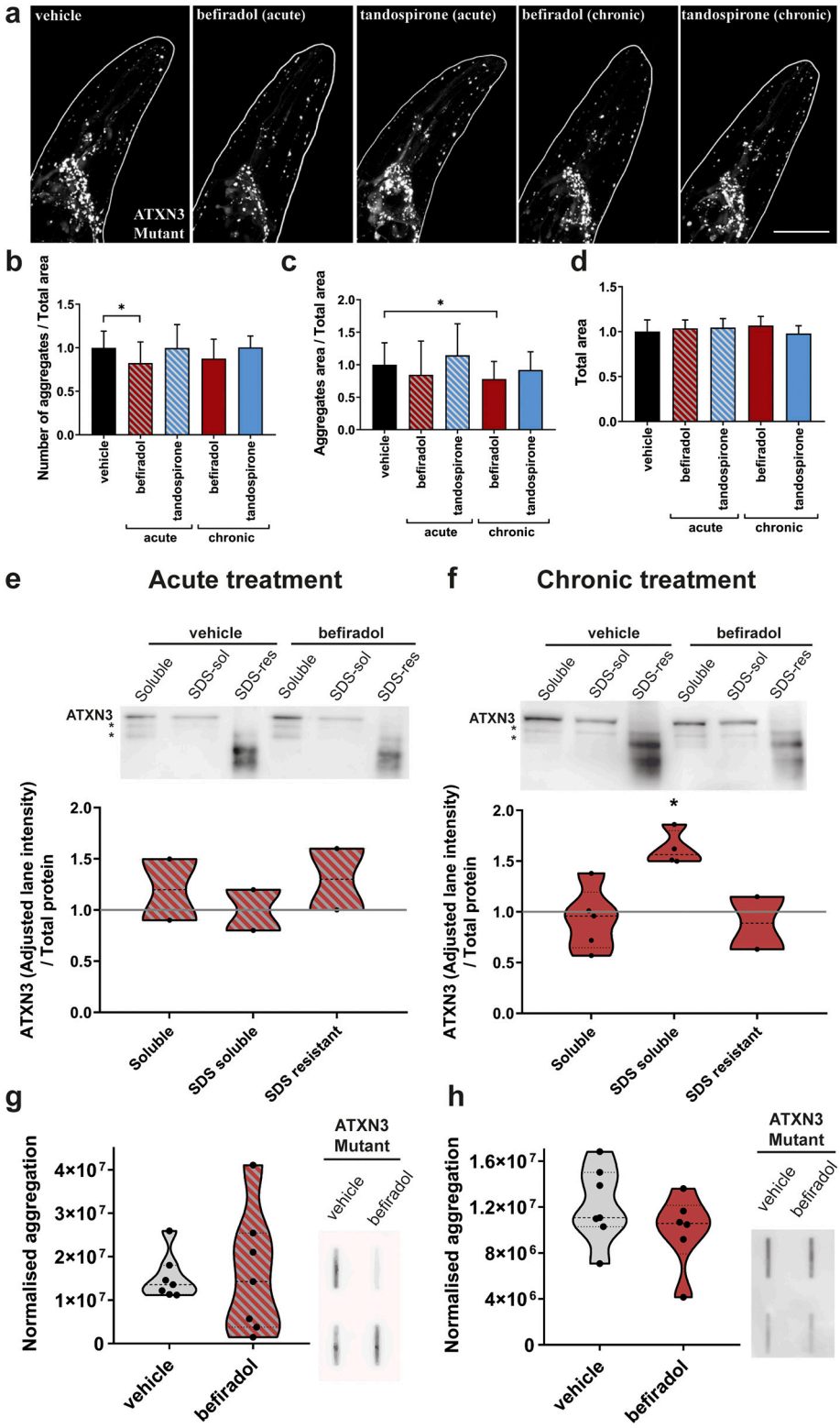


Fig. 2. Befiradol treatment decreases mutant ATXN3 aggregation. (a) Mutant ATXN3 expression pattern in the animals' head upon treatment, obtained by confocal live imaging. Scale bar: 100 μm. (b) Number of aggregates and (c) area of aggregates was decreased upon acute and chronic treatments with befiradol, respectively, with no changes in (d) total area of the animal's heads. Biochemical fractionation assay of AT3q130 (ATXN3 mutant) animals upon (f) chronic administration of the drug increases the ATXN3 species soluble in SDS. (e) Upon acute administration of befiradol no differences were found in solubility of mutant ATXN3. Filter trap retardation assay of AT3q130 (ATXN3 mutant) upon (g) acute or (h) chronic administration of befiradol. For confocal microscopy live imaging: ($n = 11–37$, ± SD – pool of 3 individual experiments), *P < 0·05 (Kruskal-Wallis with Dunn post-hoc test or One-Way ANOVA with Dunnett post-hoc test or *t*-test). For filter trap: ATXN3 densitometry values were divided by the total amount of protein measures by AzureRed®, Azure Biosystems. (n = 6–8, Q1 – Q2 – Q3). For biochemical fractionation: ($n = 2–5$, Q1 – Q2 – Q3), *P < 0·05 (one sample t-test, with Bonferroni correction *vs* value 1).

Sidak post-hoc test with bias correction (Fig. 1a – tandospirone; Fig. 4; Fig. 5a and c; Supplementary Fig. 6). When normal distribution and homogeneity of variances failed to be verified, Kruskal-Wallis with Dunn post-hoc test was applied (Fig. 2b and c – acute and tandospirone chronic treatments; Supplementary Fig. 4a and b).

For samples with normal distribution but not displaying homogeneity of variances, Brown-Forsythe were reported and Dunnett3 post-hoc test was applied (Supplementary Fig. 2c).

Toxicity assay results were compared using a non-linear regression approach (Supplementary Fig. 1) tacking in account IC50, HillSlope and Top and Bottom values.

Detailed statistics for all experiments can be consulted at supplementary table 4.

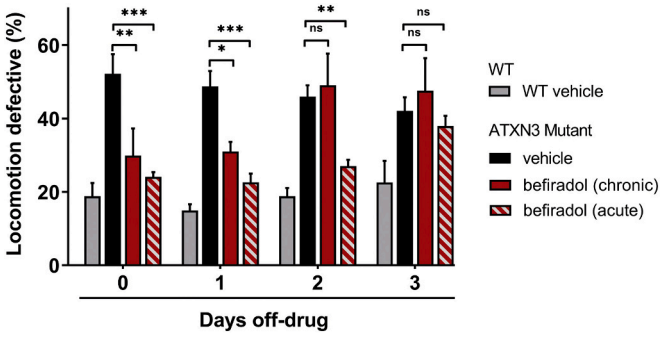


Fig. 3. Persistence of effect of befiradol treatment of ATXN3 mutant animals upon drug removal. OFF-drug effect on motor behavior of AT3q130 (ATXN3 mutant) animals treated with befiradol for either 4 days or 2 h, showing that improvements in motor performance persist at least at day 1 and day 2 post drug treatment discontinuation. After 2 days (for chronic treatment protocol) or 3 days (for acute treatment protocol) of drug withdrawal, the beneficial effect of befiradol on motor behavior declined and neurotoxicity returned. (n = 3, ± SD), *P < 0·05, **P < 0·01, ns – non-significant (Two-Way ANOVA, Tukey post-hoc test).

3. Results

3.1. Chronic and acute treatment with befiradol ameliorates mutant ATXN3-mediated neuronal dysfunction

To evaluate the impact of the activation of the 5-HT_{1A} receptor on mutant ATXN3-mediated pathogenesis, we used a *C. elegans* model of MJD proteotoxicity (ATXN3 mutant) in which the expanded form of ATXN3 (AT3q130) is expressed in neuronal cells causing progressive motor dysfunction and mutant ATXN3 aggregation (Teixeira-Castro et al., 2011a). Safe concentrations of befiradol and tandospirone to be used in subsequent assays were defined using wild-type *C. elegans* (WT, N_2) in a toxicity assay (Voisine et al., 2007). In this assay, consumption of food, assessed by the variation in the optical density of bacteria throughout time, was used as a measure of normal development and well-being of the animals. The majority of the befiradol and tandospirone concentrations tested were safe to the animals, with the exception of treatment with 500 μM of befiradol that caused a deficit in body fitness and a slight decrease in the food consumption rate (Supplementary Fig. 1). To assess motor function in *C. elegans*, we performed a motility assay where animals were placed in the centre of a plate, in the presence of food, and allowed to explore freely the environment for 1 min. After this time, the animals that did not cross 1 cm circumference were scored as motor defective. The motor index for each condition was calculated using the motor performance of wild-type ataxin-3 (ATXN3 WT, 100%) and mutant ataxin-3 (ATXN3 mutant, 0%) animals as reference. Chronic treatment of ATXN3 mutant (AT3q130) animals with befiradol or tandospirone improved motor behavior of the animals with a dose response profile and a large effect size of 0·616 and 0·605, respectively (Supplementary table 4, ω^2p). Both drugs showed a positive impact on animals' motor dysfunction in the range of concentrations of 100 nM to 100 μM, the maximum effect being obtained at 10 μM treatment (Fig. 1a). No significant differences were found in treatment efficacy between drugs. The concentration of 10 μM was used in subsequent experiments for both compounds. To further assess the impact of drug treatment on motor behavior of ATXN3 mutant animals, we evaluated an intrinsic characteristic of movement, the velocity of the animals. To do this, we filmed WT, ATXN3 WT and mutant ATXN3 animals in the presence of food, after chronic drug administration (four days). Indeed, ATXN3 mutant animals presented a decreased size-corrected speed when compared with WT animals. After chronic treatment with befiradol or tandospirone, we observed a restoration of animals' velocity (Fig. 1b). Furthermore, motility of WT or ATXN3 WT animals was not changed by any of the drug treatments, suggesting that their action specifically targets mutant ATXN3-mediated pathogenesis (Fig. 1c). To test the potential of befiradol and tandospirone treatments to revert motor impairment of adult ATXN3 mutant animals, we conducted a time course assay in which adult worms already showing core motor deficits were treated with each drug during the indicated time periods. Interestingly, acute treatment with befiradol for 2 h was sufficient to restore motor function of the animals to WT levels. In contrast, acute treatment with tandospirone did not show a statistically significant effect on motor behavior (Fig. 1d), suggesting a higher potency of befiradol for 5-HT_{1A}Rs and/or a different mode-of-action of the two drugs.

3.2. Treatment with befiradol decreases aggregation of mutant ATXN3 protein

The impact of 5-HT_{1A}R activation on mutant ATXN3 aggregation was assessed using three different techniques: *in vivo* confocal imaging, which allowed the quantification of the number and size of mutant ATXN3 *foci* (Teixeira-Castro et al., 2011a; Teixeira-Castro et al., 2011b); a biochemical fractionation assay, which discriminated ATXN3 species with distinct detergent solubilities (Koch et al., 2011); and a filter trap assay, whereby aggregates were immobilized in a cellulose acetate 0·2 μm membrane, allowing the separation of the large SDS-resistant aggregates from the soluble smaller species (Vilchez et al., 2012). Our results showed a decrease in the number or area of ATXN3 aggregates upon befiradol acute (Fig. 2a, b) and chronic (Fig. 2a, c) treatments, respectively. These changes in aggregation occurred without alteration in the ATXN3 protein steady-state levels (Supplementary Fig. 2a, b) neither in animal size, upon drug treatments (Fig. 2d). Tandospirone, however, showed limited impact on aggregation (Fig. 2a-c) in both treatment modalities. Unlike acute treatment (Fig. 2e, g), there was an increase in SDS-soluble ATXN3 species upon chronic treatment with befiradol, as assessed by biochemical fractionation (Fig. 2f). No changes were found in ATXN3 aggregation measured by filter trap (Fig. 2g, h and Supplementary Fig. 3) upon befiradol supplementation; however, blocking 5-HT re-uptake genetically (by SERT/MOD-5 ablation) significantly suppressed the levels of SDS-resistant mutant ATXN3 species, being this a positive control of the technique (Supplementary Fig. 2c). Drug efficacy was monitored in all aggregation assays by evaluating motor performance of the same animals upon treatment (Supplementary Fig. 2d). To evaluate the sustainability of drug effect after treatment withdrawal, we treated animals chronically for four days or acutely for 2 h and maintained the animals off-drug during the indicated days. Both treatment protocols maintained efficacy for at least 1 to 3 days post interruption of the treatment, further supporting a disease-modifying effect of befiradol (Fig. 3).

3.3. Befiradol acts via 5-HT_{1A}R orthologue SER-4 to mitigate motor dysfunction in C. elegans

Although with different potencies, befiradol and tandospirone are described in mammals to act as agonists of the 5-HT_{1A}R (Bollinger et al., 2010; Hamik et al., 1990; Llado-Pelfort et al., 2012). In *C. elegans*, SER-4 has been described as a putative orthologue of human 5-HT_{1A} receptors (Olde and McCombie, 1997). To verify the conservation of specific protein domains between species, we aligned human 5-HT_{1A}R (Uniprot #P08908) with SER-4 (Uniprot #G5EGH0) proteins using T-COFFEE Multiple Sequence Alignment Server (Notredame et al., 2000). Indeed, SER-4 presented a high degree of conservation of ligand binding sites and a fully conserved G-coupled protein receptor (GPCR) binding motif (DRY motif) and activation site (NPxxY motif) (Fig. 4a). The overall percentage of aminoacid similarity (Stothard, 2000) between the *C. elegans* receptor and the human 5-HTR_{1A}R is of 47·5%. The *C. elegans* serotonergic system includes at least three other GPCR: SER-1, SER-5 and SER-7, presenting high homology to human 5-HT_2R, 5-HT_6R and 5-HT_7R (Hamdan et al., 1999; Harris et al., 2009; Hobson et al., 2003),

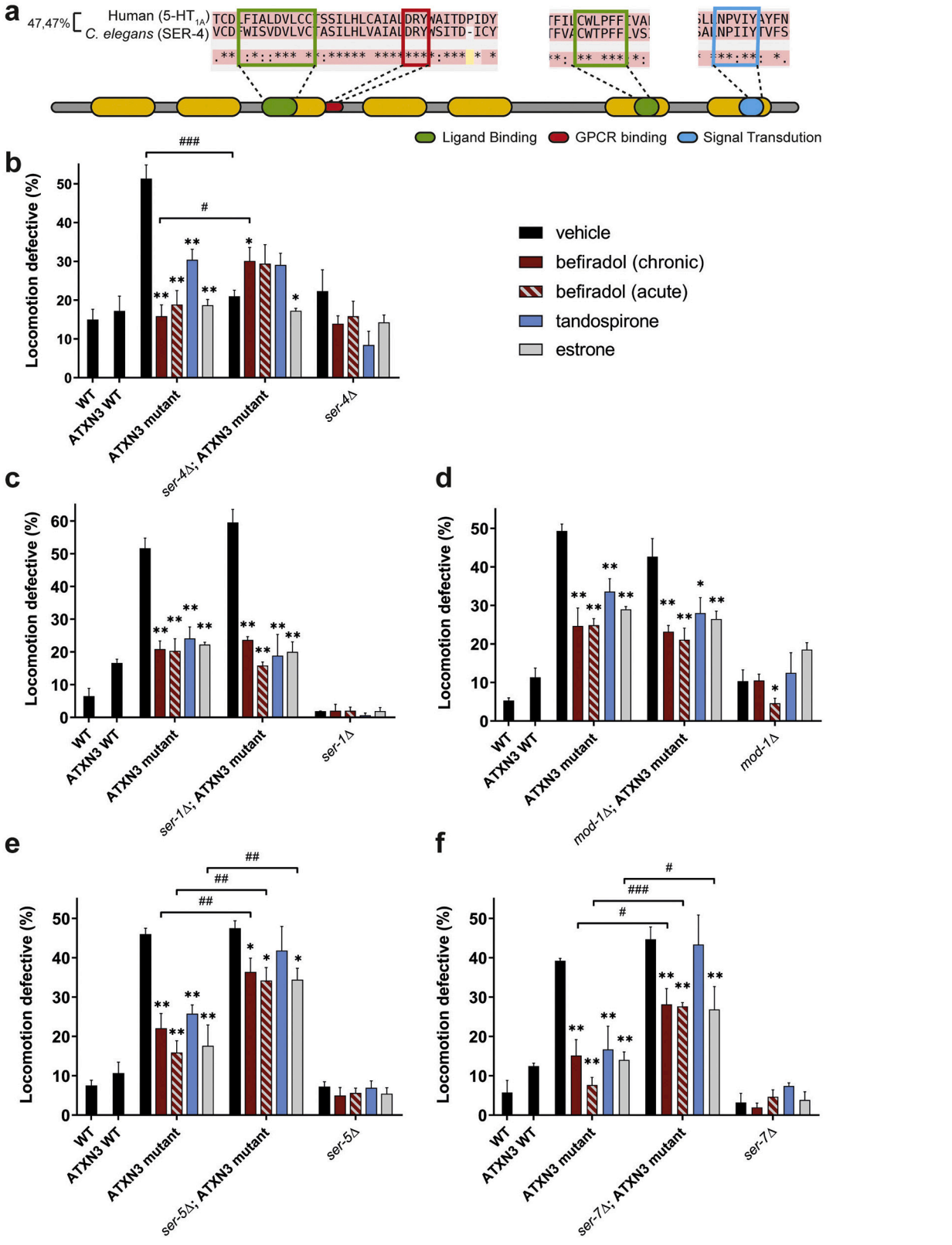


Fig. 4. *C. elegans* SER-4 receptors are molecular targets of befiradol. (a) Alignment of *Homo sapiens* (human) 5-HT_{1A}R protein with the *C. elegans* orthologue SER-4 showing conserved regions of the receptor like ligand binding motif (green), GPCR binding DRY motif (red) and signal transduction NPXXY motif (blue). Pharmacological treatment of *C. elegans* strains lacking (b) *ser-4*, (c) *ser-1*, (d) *mod-1*, (e) *ser-5* or (f) *ser-7* receptors showed that SER-4 is likely to be the molecular target of befiradol, tandospirone's effect being dependent on SER-4, SER-5 and SER-7 activity. Both drugs' action was independent of *ser-1* and *mod-1* receptors. For alignment: t-coffee multiple sequence alignment server was used (http://tcoffee.crg.cat). For pharmacogenetics: (n = 3–4, ± SD), *P < 0·05, **P < 0·01, ***P < 0·001 comparing drug treatment with vehicle, $^{\#}$P < 0·05, $^{\#\#}$P < 0·01, $^{\#\#\#}$P < 0·001 comparing strain effect within the same drug treatment (Factorial ANOVA, Sidak test corrected for BCA).

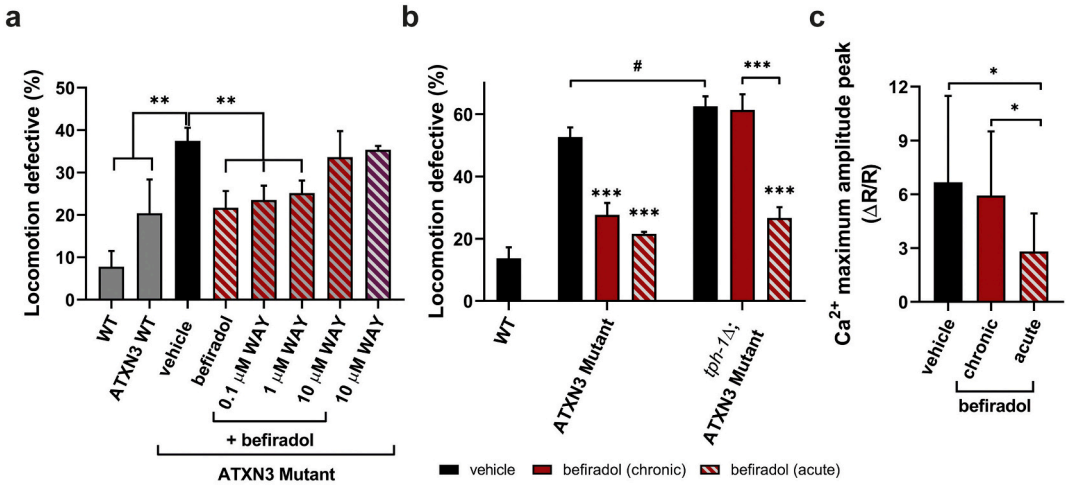


Fig. 5. 5-HT_{1A} auto- and heteroreceptors' function contribute to befiradol treatment efficacy of ATXN3 mutant animals. (a) The effect of befiradol on motor dysfunction showed to be dependent on the activation of the 5-HT_{1A} receptor. The occupation of the binding site of the receptor 5-HT_{1A} by its specific antagonist WAY 100635 precluded the effect of befiradol on mutant ATXN3-expressing animals upon acute treatment. (b) Acute befiradol treatment ameliorated motor dysfunction of mutant ATXN3 animals, even in the absence of serotonin synthesis and release, highlighting the contribution of 5-HT_{1A} heteroreceptors activation. (c) Chronic and acute administration of befiradol differently impacted HSN Ca^{2+} dynamics. Acute treatment with the drug decreased the Ca^{2+} maximum peak amplitude, which was not observed upon chronic treatment, supporting a differential response of the receptor dependent on drug treatment duration. For co-treatment (a): (n = 2–3, ± SD) **P < 0·01 (ANOVA, SIDAK test corrected for BCA). For *tph-1* pharmacogenetics (b): (n = 3, ± SD) ***P < 0·001 comparing drug treatment with vehicle, #P < 0·05 comparing strain effect within the same drug treatment (ANOVA, SIDAK test). For HSN calcium dynamics (c): (n = 11–12, ± SD) *P < 0·05 (ANOVA, SIDAK test corrected for BCA).

respectively; and one chloride channel gate receptor, MOD-1, exclusive of the *C. elegans* genome (Ranganathan et al., 2000).

To investigate the molecular targets of befiradol and of tandospirone in *C. elegans* and their role in the suppression of mutant ATXN3-mediated toxicity, we generated double mutant strains with ablation of the individual 5-HT receptors in the ATXN3 mutant background. The ablation of *ser-4* receptor reduced locomotion impairments of transgenic ATXN3 mutant animals (Fig. 4b), as previously described (Teixeira-Castro et al., 2015). This is consistent with its role as autoreceptor, loss and/or desensitization of which would lead to a disinhibition of serotonin production and release (Teixeira-Castro et al., 2015). No compensatory effects in mRNA expression level of the other serotonergic receptors were observed in *ser-4* mutant strains (Supplementary Fig. 4). By combining compound treatment with genetic tools, we found that befiradol and tandospirone treatments did not further improve motor performance of the animals, compatible with SER-4 receptors being cellular targets of both drugs. In contrast, treatment of *ser-4Δ*; ATXN3 mutant animals with estrone (a steroid hormone) was able to cause a further reduction in their motility impairment, consistent with an independent mechanism-of-action for this compound (Fig. 4b). Ablation of *ser-1* and of *mod-1* genes, however, did not have an impact on drug action for any of the compounds and treatment modalities (Fig. 4c and d). The role of SER-5/5-HT_6 and SER-7/5-HT_7 receptors in mutant ATXN3-mediated proteotoxicity discriminated the mode-of-action of the two compounds (Fig. 4e and f). Ablation of SER-5 and SER-7 precluded tandospirone-mediated amelioration of motor performance of ATXN3 mutant animals, in contrast with befiradol that still maintained its therapeutic action. The partial loss of efficacy of befiradol in the absence of SER-5 and SER-7 is mirrored upon estrone treatment, as well as with 17-DMAG and CCI779 treatments, two drugs with well-defined molecular targets (HSP90 and mTORC1 complex, respectively (Mellatyar et al., 2018; Peralba et al., 2003)) (Supplementary Fig. 5), possibly suggesting an intrinsic effect in the double mutants independent of drug action. Despite of these observations, a partial contribution of SER-5 and SER-7 receptors in befiradol action cannot be excluded. The potential drug interaction with dopaminergic signaling pathways, mostly proposed for tandospirone (Hamik et al., 1990), fails to impact on mutant ATXN3-mediated proteotoxicity (Supplementary Fig. 6). Taken together, these results support the idea that befiradol is mitigating motor dysfunction and aggregation in the *C. elegans* model of ATXN3 proteotoxicity through selective targeting of the 5-HT_{1A}R. This hypothesis was further supported by the co-treatment of ATXN3 mutant animals with befiradol and WAY-100635. WAY-100635 is a potent and selective 5-HT_{1A} antagonist (Gozlan et al., 1995; Laporte et al., 1994; Mathis et al., 1994), that upon acute administration occupies the ligand binding site of 5-HT_{1A}R without altering 5-HT release (Gurling et al., 1994). Upon administration of befiradol alone and in combination with increasing dosages of WAY 100635, we observed a dose-dependent loss of befiradol effect on the amelioration of motor dysfunction of ATXN3 mutant animals, suggesting a direct competition for the 5-HT_{1A}R ligand binding site (Fig. 5a).

3.4. Addressing 5HT_{1A} auto- and heteroreceptor contribution to befiradol's therapeutic action

The role of 5HT_{1A} auto- and heteroreceptors on mutant ATXN3 proteotoxicity was examined using pharmacogenetic approaches (Fig. 5b). Genetic ablation of the 5-HT_{1A}R orthologue SER-4 led to a suppression in proteotoxicity of mutant ATXN3-expressing animals (Fig. 4b), possibly consistent with a net effect of abrogation of the negative regulation of serotonin production mediated by autoreceptors located at serotonergic neurons. Next, we asked whether the 5-HT_{1A} heteroreceptors activity could also contribute to the effect of the drug. We tested this hypothesis by ablating the *tph-1* gene in ATXN3 mutant background. TPH-1 is the orthologue of human tryptophan hydroxylase 1 (Sze et al., 2000), the enzyme responsible for the first step of 5-HT biosynthesis, limiting the rate conversion of tryptophan into 5-HT. In *C. elegans*, a null mutation on the *tph-1* gene, the sole tryptophan hydroxylase enzyme, abolishes all 5-HT production (Sze et al., 2000), therefore making the modulatory role of 5-HT_{1A} autoreceptors on 5-HT synthesis irrelevant, but still allowing activation of 5-HT_{1A} heteroreceptors and of their downstream signaling pathways by exogenous agonists. Importantly for the mechanism of action of befiradol, upon acute treatment with this drug there was an amelioration of motor dysfunction of ATXN3 mutant animals, both in the presence or absence of TPH-1. In contrast, upon chronic administration, befiradol showed a

limited impact on the motor behavior of *tph-1Δ*; ATXN3 mutant animals (Fig. 5b). These results suggest that the beneficial effect of befiradol chronic treatment is predominantly dependent on 5-HT_{1A} autoreceptor function, likely by desensitization of these receptors in serotonergic neurons and disinhibition of serotonin release, whereas acute treatment may predominantly act through activation of the heteroreceptors in non-serotonergic neurons even in the absence of endogenous serotonin, culminating in the suppression of mutant ATXN3-associated phenotypes (Fig. 6). This is consistent with the differential impact caused by chronic or acute administration of befiradol on Ca^{2+} dynamics of HSN neurons (Fig. 5c and Supplementary Fig. 7). While acute treatment elicited a decrease in HSN activity, chronic treatment failed to do so, suggesting a desensitization of the receptor.

4. Discussion

In this study, we evaluated befiradol, a novel 5-HT_{1A} receptor full agonist, as a potential modulator of MJD pathogenesis, comparing its effects with tandospirone, a 5-HT_{1A}R partial agonist, using a *C. elegans* model of mutant ATXN3 proteotoxicity. Our results showed that befiradol treatment ameliorates core pathological features in this model, including mutant ATXN3-mediated motor dysfunction and protein aggregation in neurons upon chronic and acute administration. Hence, we propose befiradol as a disease-modifying agent and the 5-HT_{1A}R as a therapeutic target for MJD. Comparing its effect with tandospirone, befiradol presents higher potency, notably at acute administration, and high target specificity, its therapeutic effect being likely dependent on 5-

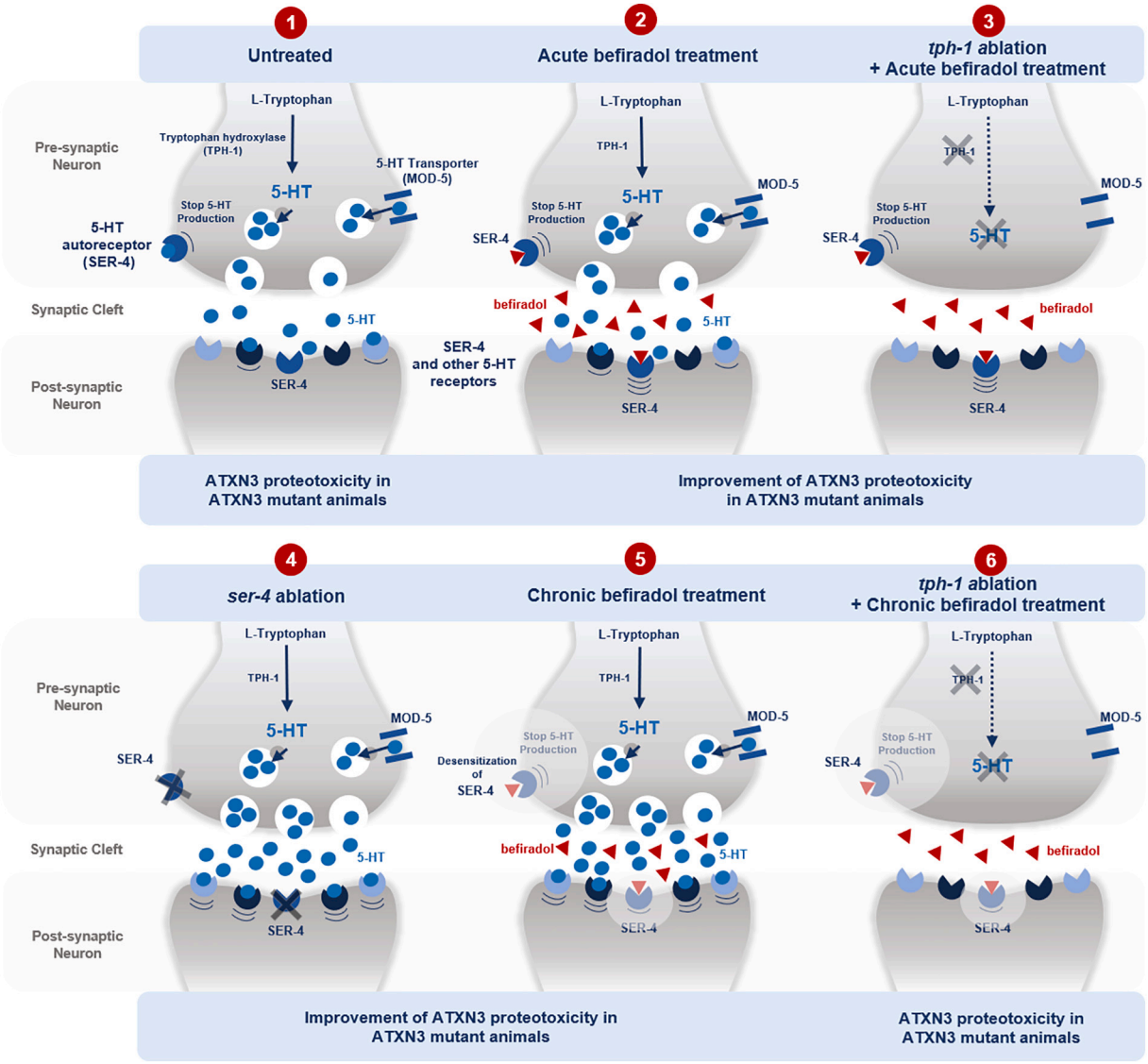


Fig. 6. Hypothetical model of befiradol action in a *C. elegans* model of ATXN3 proteotoxicity. Schematic of serotonergic synapses showing that 5-HT is synthesized and released into the synaptic cleft, where it activates postsynaptic 5-HT receptors, activating the regulatory signaling coupled with the different 5-HT hetero-receptors. Serotonin also binds the 5-HT autoreceptor SER-4, eliciting the "stop 5-HT production" signal mediated by 5-HT autoreceptors in presynaptic neurons (1). Acute treatment with befiradol rapidly targeted 5-HT_{1A}/SER-4 receptors, activating protective cellular pathways against mutant ATXN3-mediated neuronal dysfunction (2). In the absence of endogenous serotonin, through ablation of the *tph-1* gene, acute treatment with befiradol still improved motor function, suggesting a contribution of 5-HT_{1A} hetero-receptors signaling for the suppression of mutant ATXN3-associated phenotypes (3). *ser-4* ablation also suppressed proteotoxicity, consistent with a possible disinhibition of serotonin synthesis and release, likely increasing its availability, as described previously for chronic treatment with selective serotonin re-uptake inhibitors (4). Chronic treatment with befiradol suppressed mutant ATXN3 pathogenesis through activation of 5-HT_{1A}/SER-4 receptors, an effect which we hypothesize includes the disinhibition of serotonin release, likely by desensitization of the 5-HT_{1A}/SER-4 auto-receptor at the pre-synapse (5). In the absence of endogenous serotonin, through ablation of the *tph-1* gene, chronic treatment with befiradol was insufficient to suppress ATXN3 proteotoxicity, further supporting a possible role of the disinhibition of serotonin release upon chronic treatment with befiradol (6).

HT_{1A} auto- and hetero-receptors (Fig. 6).

Pharmacologic and genetic modulation of serotonergic signaling was previously shown to impact MJD pathogenesis, being able to suppress mutant ATXN3 aggregation and to restore motor function in three distinct MJD animal models exposed to chronic administration of citalopram (Ashraf et al., 2019; Esteves et al., 2019; Teixeira-Castro et al., 2015). Interestingly, this effect was dependent not only of SERT/MOD-5, the citalopram molecular target, but also on the 5-HT_{1A}/SER-4 and 5-HT_2/SER-1 receptors (Teixeira-Castro et al., 2015). Although the mechanism of action of citalopram is not fully understood, there is evidence that the therapeutic effects of SSRIs are modulated by 5-HT_{1A}R function (Kulikov et al., 2018; Stahl, 1998). Specifically, citalopram chronic treatment was shown to lead to 5-HT_{1A} auto-receptor desensitization, increasing 5-HT availability (Invernizzi et al., 1994), and to increase the functional sensitivity of post-synaptic 5-HT_{1A} hetero-receptors (Moulin-Sallanon et al., 2009). In addition, enhancement of the signaling cascades downstream of 5-HT_{1A}R, upon chronic citalopram treatment and direct targeting of 5-HT_{1A}R, has a modulatory effect on glutamatergic (Cervantes-Ramirez et al., 2019), dopaminergic and noradrenergic signaling pathways, further supporting a broad and overarching mode-of-action of the serotonergic system in the brain (Kaneko et al., 2016). The adaptation of the serotonergic system, in particular 5-HT_{1A}R desensitization, needed for citalopram action, could explain the delay in phenotypic amelioration seen in depression upon treatment with this drug. Often, patients with major depression discontinue citalopram use due to anxiety symptoms in the first weeks of treatment, this emotional imbalance being associated with 5-HT_{1A}R activation at the Dorsal Raphe Nucleus (DRN), as seen in a PET and functional MRI study (Selvaraj et al., 2018). This close relationship between citalopram action and 5-HT_{1A} receptor signaling further supported the hypothesis that direct modulation of 5-HT_{1A}Rs could suppress MJD pathogenesis. Indeed, previous studies in patients showed efficacy of two 5-HT_{1A}R agonists, buspirone and tandospirone, in amelioration of cerebellar ataxia symptomatology (Ogawa, 2004; Takei et al., 2005). Buspirone led to an improvement of clinical and self-assessment test scores in patients with cerebellar cortical atrophy and olivopontocerebellar atrophy (Lou et al., 1995), however this effect was shown to be partial and not major (Trouillas et al., 1997). Tandospirone treatment improved the ataxia rating scale (ARS) scores in MJD and SCA6 patients (Takei et al., 2010). In the MJD cohort, patients showed improved gait, posture, kinetic and total ARS during the 3 to 4 weeks of treatment (Takei et al., 2004). However, the withdrawal of tandospirone reverted symptom amelioration, showing a non-modulatory short-term effect of tandospirone treatment in MJD pathogenesis (Takei et al., 2004). Interestingly, buspirone and tandospirone were classified as partial agonists of 5-HT_{1A} hetero-receptors (Huang et al., 2017; Yocca, 1990), making it plausible that a potent and selective 5-HT_{1A}R agonist (Colpaert et al., 2002) might increase efficacy. Accordingly, this study shows that although befiradol elicited the same effect size as tandospirone upon chronic treatment, befiradol also suppressed MJD pathogenesis on acute administration, contrary to tandospirone. This is consistent with the description of tandospirone as a partial agonist of 5-HT_{1A} hetero-receptors and with the primary effect of acute treatment with befiradol being predominantly mediated by the activation of 5-HT_{1A} hetero-receptors and independent of the serotonin synthesis downregulation signal mediated by autoreceptors. In addition to a decreased agonism effect (60%) compared to a selective 5-HT_{1A} agonist (Hamik et al., 1990), tandospirone may also be a suboptimal therapeutic agent in view of its interactions with multiple cellular targets, namely serotonin 5-HT_2, dopamine D_2 and alpha-adrenergic receptors, which our data suggest are not essential for the therapeutic effects of 5-HT_{1A}R-targeting drugs in MJD.

The pattern of binding and activation by befiradol in the brain has been extensively studied in rat, cat, macaque and, more recently, in human using a variety of *in vitro*, *ex vivo*, PET imaging and fMRI techniques (Bardin et al., 2005; Colom et al., 2020; Levigoureux et al., 2019; Llado-Pelfort et al., 2012; Vidal et al., 2019; Vidal et al., 2018). Since the 5-HT_{1A}R is highly expressed in the DRN, the serotonergic core of the brain, not surprisingly, befiradol binds to the 5-HT_{1A} autoreceptors of DRN neurons (Levigoureux et al., 2019; Vidal et al., 2019; Vidal et al., 2018) and decreases the neuronal firing rate (Llado-Pelfort et al., 2012) through activation of the negative feedback loop of serotonin production. The desensitization of these autoreceptors is probably accounting for the effect of befiradol chronic treatment in mutant ATXN3-expressing animals, by increasing serotonin availability (Fig. 6). However, befiradol not only activates 5-HT_{1A} autoreceptors but also heteroreceptors (Llado-Pelfort et al., 2012). Extensive PET/fRMI studies, using several species, showed activity of befiradol for thalamus, cingulate cortex and hippocampus (Vidal et al., 2019; Vidal et al., 2018), the receptor occupancy being correlated with changes in activation of these regions, and in the occipital lobe, amygdala, sub-regions of the brainstem and right motor cortex (Vidal et al., 2018). A study with conscious rats showed a more detailed pattern of befiradol binding-selectivity with activation of the pontine nuclei and cerebellum, and an inhibition in the brainstem, piriform cortex and striatum (Levigoureux et al., 2019). Some of these areas have been described as atrophic or damaged in MJD, like the thalamus (Paulson, 2012), and cerebellar–thalamocortical and basal ganglia–thalamocortical pathways (Wang et al., 2020a), or related with ataxic dysfunction and severity, including the cingulate cortex, cerebellum (Hernandez-Castillo et al., 2017) and brainstem (Jafari et al., 2011).

In *C. elegans*, serotonin is present in eight classes of neurons: NSM, HSN, $VC_{4,5}$, ADF, RIH and AIM (Chase and Koelle, 2007), the production of serotonin occurring in NSM, HSN and ADF neurons (Horvitz et al., 1982; Jafari et al., 2011). As in the vertebrate brain, these serotonin-producing neurons project to and regulate non-serotonergic cells that express serotonin receptors. The effect of befiradol proved to be dependent on SER-4, the 5-HT_{1A} orthologue (Olde and McCombie, 1997), which is expressed in neurons, like serotonergic neuron NSM (Gurel et al., 2012), cholinergic (RIB and DVA), glutamatergic (DVC and AIB) and GABAergic (RIS) interneurons (Gurel et al., 2012; Tsalik et al., 2003), but also in a type II vulval muscle cell (vm2) (Gurel et al., 2012; Ravi et al., 2018a), SER-4 expression being required for the effects of endogenous serotonin in locomotion (Gurel et al., 2012).

Importantly, the suppression of ATXN3 aggregation caused by pharmacological modulation of the serotonergic system by citalopram (Ashraf et al., 2019; Teixeira-Castro et al., 2015) and befiradol treatment (this work) are mimicked by genetic ablation of their respective cellular targets. Their effect on protein folding and aggregation suggests that protein homeostasis mechanism(s) may be a link between serotonergic signaling and neurodegeneration associated with proteotoxicity. The exact mechanism of proteostasis modulation by serotonin is unknown, however some candidate pathways have been proposed. HSP90 inhibition improved balance and motor coordination of a MJD mice model (Silva-Fernandes et al., 2014), and the abundance of Hsp90β was directly correlated with ATXN3 high molecular weight species upon citalopram treatment (Ashraf et al., 2019). Interestingly, serotonin was shown to be indispensable for inter-tissue or non-cell autonomous communication of the folding status of an organism (Berendzen et al., 2016; Tatum et al., 2015; Zhang et al., 2018). In this process, the proteotoxic stress caused by the expression of mutant polyQ proteins in neuronal cells was communicated to distal tissues to improve organism proteostasis *via* the activation of the unfolded protein response of mitochondria (UPR^{mt}) (Berendzen et al., 2016). This communication was found to occur *via* WNT signaling and to require serotonin release from serotonergic neurons (Zhang et al., 2018), further supporting that serotonin regulates protein homeostasis at an inter-cellular level. The modulation of protein homeostasis upon serotonergic signaling activation could, therefore, have a positive impact not only on MJD pathogenesis but also in other proteinopathies, such as Parkinson's Disease (PD) and Alzheimer's Disease (AD) (Bayer, 2015; Ross and Poirier, 2004). Indeed, serotonergic signaling dysfunction was recently reported

in PD (Fazio et al., 2020), ALS (reviewed in (Vermeiren et al., 2018)) and AD (Pena-Bautista et al., 2020; Snowden et al., 2019). Interestingly, AD patients present low SERT binding in the limbic regions of the brain (van der Zande et al., 2020) and decreased expression of 5-HT_{1A} receptor (Lanctot et al., 2007). It has been shown that serotonergic signaling modulation by tandospirone (Sato et al., 2007), citalopram (Meyer et al., 2019) or its enantiomer escitalopram impacts on AD pathogenesis (Wang et al., 2016). Interestingly, escitalopram attenuated beta-amyloid-induced tau hyperphosphorylation through 5-HT_{1A} receptor-mediated Akt/GSK-3β pathway (Wang et al., 2020b; Wang et al., 2016), possibly underlying the beneficial effects seen in cognition of AD and vascular dementia patients (Ramirez et al., 2014; Xie et al., 2019). In PD, befiradol treatment reverted L-DOPA-induced dyskinesia (Depoortere et al., 2020; Iderberg et al., 2015; McCreary et al., 2016), a side-effect caused by prolonged administration of L-DOPA. 5-HT_{1A}R agonism and befiradol treatment very efficaciously activated inhibitory somatodendritic 5-HT_{1A} autoreceptors in the DRN. This decreases 5-HT release and blocks the "false neurotransmitter" surge of DA release elicited by L-DOPA administration from 5-HT neurons — an effect that underlies the potent antidyskinetic action of befiradol. Befiradol also activated cortical 5-HT_{1A} heteroreceptors, which can be associated with the beneficial properties seen in models of mood and cognition deficits (Iderberg et al., 2015). Recently, it was found that befiradol can have some anti-parkinsonism properties in MPTP-treated macaques (Fisher et al., 2020), coherent with the findings that 5-HT_{1A}R agonism, by 8-OH-DPAT or buspirone, ameliorated haloperidol-induced catalepsy and bradykinesia (Mohajjel Nayebi and Sheidaei, 2010; Ohno et al., 2008). Therefore, serotonergic signaling stimulation seems to be also effective for parkinsonism, L-DOPA-induced dyskinesia, cognitive impairment and neurodegeneration of dopaminergic neurons (Ohno, 2011; Ohno et al., 2015).

In conclusion, our results strengthen interest in the modulation of serotonergic signaling as a promising therapeutic approach for MJD, presenting befiradol as a potent and selective 5-HT_{1A}R agonist *in vivo*. In the future, in-depth studies and translational analysis using MJD mouse models will be required to further validate befiradol use as therapeutic agent and to dissect the involvement of 5-HT_{1A} receptors signaling in the suppression of MJD pathogenesis.

Contributors

J.P-S, A.T-C and P.M. contributed to the study design. J.P-S, B.F-L, A. B-S, D.V-C, J.H.F, M.D.C and A.T-C collected the data. Interpretation of data was made by J.P-S, A.T-C and P.M. The first draft was written by J. P-S, which was critically commented by A.T-C, A.N-T, M.A.V. and P.M. All authors revised and approved the final version of the manuscript.

Data sharing statement

Data sets can be shared by request to the corresponding author.

Declaration of interests

J.P-S, B.F-L, A.B-S, D.V-C, J.H.F, M.D.C, A.T-C, P.M declare no conflict of interest. Mark A. Varney, Adrian Newman-Tancredi are stockholders of Neurolixis.

Acknowledgements

We are grateful to members of the Maciel laboratory for sharing reagents, for critical analysis of the data and discussions on the manuscript. Thanks to the Caenorhabditis Genetics Center (CGC), which is funded by NIH Office of Research Infrastructure Programs (P40 OD010440), and to National Bioresource Project for the Experimental Animal "Nematode *C. elegans*" (NBRP) for providing some of the nematode strains used in this study.

This work was funded by FEDER, through the Competitiveness Internationalization Operational Programme (POCI), and by National funds, through the Foundation for Science and Technology (FCT), under the scope of the project POCI-01-0145-FEDER-0 31987, NORTE-01-0145-FEDER-000013 and NORTE-01-0145-FEDER-000023, supported by the Northern Portugal Regional Operational Programme (NORTE 2020), under the Portugal 2020 Partnership Agreement, through the European Regional Development Fund (ERDF) and by ICVS Scientific Microscopy Platform, member of the national infrastructure PPBI - Portuguese Platform of Bioimaging (PPBI-POCI-01-0145-FEDER-022122); by National funds, through the Foundation for Science and Technology (FCT) - project UIDB/50026/2020 and UIDP/50026/2020. Additionally, this project was supported by National Ataxia Foundation (NAF) and the FCT individual fellowship PD/BDE/127834/2016 (For J. P-S).

Appendix A. Supplementary data

Supplementary data to this article can be found online at https://doi.org/10.1016/j.nbd.2021.105278.

References

Albert, P.R., Vahid-Ansari, F., 2019. The 5-HT1A receptor: signaling to behavior. Biochimie. 161, 34–45.
Albert, P.R., et al., 1990. Cloning, functional expression, and mRNA tissue distribution of the rat 5-hydroxytryptamine1A receptor gene. J. Biol. Chem. 265, 5825–5832.
Ashraf, N.S., et al., 2019. Citalopram reduces aggregation of ATXN3 in a YAC transgenic mouse model of Machado-Joseph disease. Mol. Neurobiol. 56, 3690–3701.
Bardin, L., et al., 2005. Dual, hyperalgesic, and analgesic effects of the high-efficacy 5-hydroxytryptamine 1A (5-HT1A) agonist F 13640 [(3-chloro-4-fluoro-phenyl)-[4-fluoro-4-{[(5-methyl-pyridin-2-ylmethyl)-amino]-me thyl}piperidin-1-yl] methanone, fumaric acid salt]: relationship with 5-HT1A receptor occupancy and kinetic parameters. J. Pharmacol. Exp. Ther. 312, 1034–1042.
Bayer, T.A., 2015. Proteinopathies, a core concept for understanding and ultimately treating degenerative disorders? Eur. Neuropsychopharmacol. 25, 713–724.
Berends, A.C., et al., 2005. A review of the neuroprotective properties of the 5-HT1A receptor agonist repinotan HCl (BAYx3702) in ischemic stroke. CNS Drug Rev. 11, 379–402.
Berendzen, K.M., et al., 2016. Neuroendocrine coordination of mitochondrial stress signaling and proteostasis. Cell. 166 (1553–1563), e10.
Bollinger, S., et al., 2010. Novel pyridylmethylamines as highly selective 5-HT(1A) superagonists. J. Med. Chem. 53, 7167–7179.
Brenner, S., 1974. The genetics of *Caenorhabditis elegans*. Genetics. 77, 71–94.
Cervantes-Ramirez, V., et al., 2019. Citalopram reduces glutamatergic synaptic transmission in the auditory cortex via activation of 5-HT1A receptors. Neuroreport. 30, 1316–1322.
Chase, D.L., Koelle, M.R., 2007. Biogenic amine neurotransmitters in *C. elegans*. In: WormBook, pp. 1–15.
Collins, K.M., et al., 2016. Activity of the *C. elegans* egg-laying behavior circuit is controlled by competing activation and feedback inhibition. Elife 5.
Colom, M., et al., 2020. (18)F-F13640 PET imaging of functional receptors in humans. Eur. J. Nucl. Med. Mol. Imaging 47, 220–221.
Colpaert, F.C., et al., 2002. Large-amplitude 5-HT1A receptor activation: a new mechanism of profound, central analgesia. Neuropharmacology. 43, 945–958.
Costa, M.D.C., et al., 2016. Unbiased screen identifies aripiprazole as a modulator of abundance of the polyglutamine disease protein, ataxin-3. Brain. 139, 2891–2908.
Da Silva, J.D., et al., 2019. From pathogenesis to novel therapeutics for spinocerebellar ataxia type 3: evading potholes on the way to translation. Neurotherapeutics. 16, 1009–1031.
Depoortere, R., et al., 2020. The selective 5-HT1A receptor agonist, NLX-112, exerts anti-dyskinetic effects in MPTP-treated macaques. Parkinsonism Relat. Disord. 78, 151–157.
Druse, M., et al., 2005. Signaling pathways involved with serotonin1A agonist-mediated neuroprotection against ethanol-induced apoptosis of fetal rhombencephalic neurons. Brain Res. Dev. Brain Res. 159, 18–28.
Duarte-Neves, J., et al., 2015. Neuropeptide Y mitigates neuropathology and motor deficits in mouse models of Machado-Joseph disease. Hum. Mol. Genet. 24, 5451–5463.
Esteves, S., et al., 2019. Preclinical evidence supporting early initiation of citalopram treatment in Machado-Joseph disease. Mol. Neurobiol. 56, 3626–3637.
EU_Clinical_Trials, 2009. EU Clinical Trials Register [Internet]: Amsterdam: European Medicines Agency (EU): Identifier EUCTR2009-012123-28. A Dose-finding Study of Efficacy and Safety of F13640 in Patients With Moderate to Severe Painful Peripheral Diabetic Polyneuropathy. https://www.clinicaltrialsregister.eu/ctr-search/search?query=2009-012123-28. (Accessed September 2020).
Fazio, P., Ferreira, D., Svenningsson, P., et al., 2020. High-resolution PET imaging reveals subtle impairment of the serotonin transporter in an early non-depressed

Parkinson's disease cohort. Eur. J. Nucl. Med. Mol. Imaging 47, 2407–2416. https://doi.org/10.1007/s00259-020-04683-4.
Fisher, R., et al., 2020. The selective 5-HT1A receptor agonist, NLX-112, exerts anti-dyskinetic and anti-parkinsonian-like effects in MPTP-treated marmosets. Neuropharmacology. 167, 107997.
Garcia-Garcia, A.L., et al., 2014. 5-HT(1A) [corrected] receptors in mood and anxiety: recent insights into autoreceptor versus heteroreceptor function. Psychopharmacology 231, 623–636.
Gidalevitz, T., et al., 2009. Destabilizing protein polymorphisms in the genetic background direct phenotypic expression of mutant SOD1 toxicity. PLoS Genet. 5, e1000399.
Goncalves, N., et al., 2017. Caffeine alleviates progressive motor deficits in a transgenic mouse model of spinocerebellar ataxia. Ann. Neurol. 81, 407–418.
Gozlan, H., et al., 1995. The selective 5-HT1A antagonist radioligand [3H]WAY 100635 labels both G-protein-coupled and free 5-HT1A receptors in rat brain membranes. Eur. J. Pharmacol. 288, 173–186.
Gurel, G., et al., 2012. Receptors and other signaling proteins required for serotonin control of locomotion in *Caenorhabditis elegans*. Genetics. 192, 1359–1371.
Gurling, J., M., A.A.-P., Dourish, C.T., Routledge, C., 1994. Effects of acute and chronic treatment with the selective 5-HT1A receptor antagonist WAY-100635 on hippocampal 5-HT release in vivo. Br. J. Pharmacol. 112, 299 P.
Hamdan, F.F., et al., 1999. Characterization of a novel serotonin receptor from *Caenorhabditis elegans*: cloning and expression of two splice variants. J. Neurochem. 72, 1372–1383.
Hamik, A., et al., 1990. Analysis of tandospirone (SM-3997) interactions with neurotransmitter receptor binding sites. Biol. Psychiatry 28, 99–109.
Harris, G.P., et al., 2009. Three distinct amine receptors operating at different levels within the locomotory circuit are each essential for the serotonergic modulation of chemosensation in *Caenorhabditis elegans*. J. Neurosci. 29, 1446–1456.
Hernandez-Castillo, C.R., et al., 2017. Neural correlates of ataxia severity in spinocerebellar ataxia type 3/Machado-Joseph disease. Cerebellum Ataxias. 4, 7.
Hobson, R.J., et al., 2003. SER-7b, a constitutively active Galphas coupled 5-HT7-like receptor expressed in the *Caenorhabditis elegans* M4 pharyngeal motorneuron. J. Neurochem. 87, 22–29.
Horvitz, H.R., et al., 1982. Serotonin and octopamine in the nematode *Caenorhabditis elegans*. Science. 216, 1012–1014.
Huang, X., et al., 2017. Role of tandospirone, a 5-HT1A receptor partial agonist, in the treatment of central nervous system disorders and the underlying mechanisms. Oncotarget. 8, 102705–102720.
Iderberg, H., et al., 2015. NLX-112, a novel 5-HT1A receptor agonist for the treatment of L-DOPA-induced dyskinesia: behavioral and neurochemical profile in rat. Exp. Neurol. 271, 335–350.
Invernizzi, R.W., et al., 1988. 8-Hydroxy-2-(di-n-propylamino) tetralin, a selective serotonin1A receptor agonist, blocks haloperidol-induced catalepsy by an action on raphe nuclei medianus and dorsalis. Neuropharmacology. 27, 515–518.
Invernizzi, R., et al., 1994. Chronic treatment with citalopram facilitates the effect of a challenge dose on cortical serotonin output: role of presynaptic 5-HT1A receptors. Eur. J. Pharmacol. 260, 243–246.
Jafari, G., et al., 2011. Regulation of extrasynaptic 5-HT by serotonin reuptake transporter function in 5-HT-absorbing neurons underscores adaptation behavior in *Caenorhabditis elegans*. J. Neurosci. 31, 8948–8957.
Kaneko, F., et al., 2016. Long-term citalopram treatment alters the stress responses of the cortical dopamine and noradrenaline systems: the role of cortical 5-HT1A receptors. Int. J. Neuropsychopharmacol. 19.
Kawaguchi, Y., et al., 1994. CAG expansions in a novel gene for Machado-Joseph disease at chromosome 14q32.1. Nat. Genet. 8, 221–228.
Kia, H.K., et al., 1996. Immunocytochemical localization of serotonin1A receptors in the rat central nervous system. J. Comp. Neurol. 365, 289–305.
Koch, P., et al., 2011. Excitation-induced ataxin-3 aggregation in neurons from patients with Machado-Joseph disease. Nature. 480, 543–546.
Kulikov, A.V., et al., 2018. Interplay between the key proteins of serotonin system in SSRI antidepressants efficacy. Expert Opin. Ther. Targets 22, 319–330.
Lanctot, K.L., et al., 2007. A positron emission tomography study of 5-hydroxytryptamine-1A receptors in Alzheimer disease. Am. J. Geriatr. Psychiatry 15, 888–898.
Laporte, A.M., et al., 1994. Selective in vivo labelling of brain 5-HT1A receptors by [3H] WAY 100635 in the mouse. Eur. J. Pharmacol. 271, 505–514.
Levigoureux, E., et al., 2019. Serotonin 5-HT1A receptor biased agonists induce different cerebral metabolic responses: a [(18)F]-fluorodesoxyglucose positron emission tomography study in conscious and anesthetized rats. ACS Chem. Neurosci. 10, 3108–3119.
Livak, K.J., Schmittgen, T.D., 2001. Analysis of relative gene expression data using real-time quantitative PCR and the 2(-Delta Delta C(T)) method. Methods. 25, 402–408.
Llado-Pelfort, L., et al., 2012. In vivo electrophysiological and neurochemical effects of the selective 5-HT1A receptor agonist, F13640, at pre- and postsynaptic 5-HT1A receptors in the rat. Psychopharmacology 221, 261–272.
Lou, J.S., et al., 1995. Use of buspirone for treatment of cerebellar ataxia. An open-label study. Arch. Neurol. 52, 982–988.
Mathis, C.A., et al., 1994. [11C]WAY 100635: a radioligand for imaging 5-HT1A receptors with positron emission tomography. Life Sci. 55, PL403–7.
McCreary, A.C., et al., 2016. The novel 5-HT1A receptor agonist, NLX-112 reduces l-DOPA-induced abnormal involuntary movements in rat: a chronic administration study with microdialysis measurements. Neuropharmacology. 105, 651–660.
Mellatyar, H., et al., 2018. Targeted cancer therapy through 17-DMAG as an Hsp90 inhibitor: overview and current state of the art. Biomed. Pharmacother. 102, 608–617.
Mello, C.C., et al., 1991. Efficient gene transfer in C.elegans: extrachromosomal maintenance and integration of transforming sequences. EMBO J. 10, 3959–3970.
Mendonca, N., et al., 2018. Clinical features of Machado-Joseph disease. Adv. Exp. Med. Biol. 1049, 255–273.
Meyer, S., et al., 2019. Citalopram improves obsessive-compulsive crossword puzzling in frontotemporal dementia. Case Rep. Neurol. 11, 94–105.
Miyazaki, I., Asanuma, M., 2016. Serotonin 1A receptors on astrocytes as a potential target for the treatment of Parkinson's disease. Curr. Med. Chem. 23, 686–700.
Mohajjel Nayebi, A.A., Sheidaei, H., 2010. Buspirone improves haloperidol-induced Parkinson disease in mice through 5-HT(1A) recaptors. Daru. 18, 41–45.
Moulin-Sallanon, M., et al., 2009. Acute and chronic effects of citalopram on 5-HT1A receptor-labeling by [18F]MPPF and -coupling to receptors-G proteins. Synapse. 63, 106–116.
Neves-Carvalho, A., et al., 2020. Polyglutamine spinocerebellar ataxias: emerging therapeutic targets. Expert Opin. Ther. Targets 24 (11), 1099–1119. https://doi.org/10.1080/14728222.2020.1827394.
Newman-Tancredi, A., et al., 2017. Distinctive in vitro signal transduction profile of NLX-112, a potent and efficacious serotonin 5-HT1A receptor agonist. J. Pharm. Pharmacol. 69, 1178–1190.
Notredame, C., et al., 2000. T-coffee: a novel method for fast and accurate multiple sequence alignment. J. Mol. Biol. 302, 205–217.
Nussbaum-Krammer, C.I., et al., 2015. Investigating the spreading and toxicity of prion-like proteins using the metazoan model organism *C. elegans*. J. Vis. Exp. 52321.
Ogawa, M., 2004. Pharmacological treatments of cerebellar ataxia. Cerebellum. 3, 107–111.
Ohno, Y., 2011. Therapeutic role of 5-HT1A receptors in the treatment of schizophrenia and Parkinson's disease. CNS Neurosci. Ther. 17, 58–65.
Ohno, Y., et al., 2008. Evaluation of the antibradykinetic actions of 5-HT1A agonists using the mouse pole test. Prog. Neuro-Psychopharmacol. Biol. Psychiatry 32, 1302–1307.
Ohno, Y., et al., 2015. New insight into the therapeutic role of the serotonergic system in Parkinson's disease. Prog. Neurobiol. 134, 104–121.
Olde, B., McCombie, W.R., 1997. Molecular cloning and functional expression of a serotonin receptor from *Caenorhabditis elegans*. J. Mol. Neurosci. 8, 53–62.
Oosterink, B.J., et al., 2003. Post-lesion administration of 5-HT1A receptor agonist 8-OH-DPAT protects cholinergic nucleus basalis neurons against NMDA excitotoxicity. Neuroreport. 14, 57–60.
Paillard, B.E., Del Frari, Laurence, Brunner, Valérie, Adrian, Newman Tancredi, Varney, Mark, 2020. Method for Treating Movement Disorders With Befiradol. Pierre Fabre Medicament (Boulogne-Billancourt, FR), United States.
Paix, A., et al., 2015. High efficiency, homology-directed genome editing in *Caenorhabditis elegans* using CRISPR-Cas9 ribonucleoprotein complexes. Genetics. 201, 47–54.
Paulson, H., 2012. Machado-Joseph disease/spinocerebellar ataxia type 3. Handb. Clin. Neurol. 103, 437–449.
Pena-Bautista, C., et al., 2020. Plasma alterations in cholinergic and serotonergic systems in early Alzheimer disease: diagnosis utility. Clin. Chim. Acta 500, 233–240.
Peralba, J.M., et al., 2003. Pharmacodynamic evaluation of CCI-779, an inhibitor of mTOR, in cancer patients. Clin. Cancer Res. 9, 2887–2892.
Pompeiano, M., et al., 1992. Distribution and cellular localization of mRNA coding for 5-HT1A receptor in the rat brain: correlation with receptor binding. J. Neurosci. 12, 440–453.
Prinssen, E.P., et al., 2002. 5-HT1A receptor activation and anti-cataleptic effects: high-efficacy agonists maximally inhibit haloperidol-induced catalepsy. Eur. J. Pharmacol. 453, 217–221.
Ramirez, M.J., et al., 2014. Serotonergic therapies for cognitive symptoms in Alzheimer's disease: rationale and current status. Drugs. 74, 729–736.
Ranganathan, R., et al., 2000. MOD-1 is a serotonin-gated chloride channel that modulates locomotory behaviour in *C. elegans*. Nature. 408, 470–475.
Ravi, B., et al., 2018a. Homeostatic feedback modulates the development of two-state patterned activity in a model serotonin motor circuit in *Caenorhabditis elegans*. J. Neurosci. 38, 6283–6298.
Ravi, B., et al., 2018 Feb 7. Ratiometric calcium imaging of individual neurons in behaving *Caenorhabditis elegans*. J. Vis. Exp. 7 (132), 56911. https://doi.org/10.3791/56911 (PMID: 29443112; PMCID: PMC5912386).
Riad, M., et al., 2000. Somatodendritic localization of 5-HT1A and preterminal axonal localization of 5-HT1B serotonin receptors in adult rat brain. J. Comp. Neurol. 417, 181–194.
Ross, C.A., Poirier, M.A., 2004. Protein aggregation and neurodegenerative disease. Nat. Med. 10 (Suppl), S10–S17.
Sato, S., et al., 2007. A preliminary open-label study of 5-HT1A partial agonist tandospirone for behavioural and psychological symptoms associated with dementia. Int. J. Neuropsychopharmacol. 10, 281–283.
Schatzberg, A.F., 2002. Pharmacological principles of antidepressant efficacy. Hum. Psychopharmacol. 17 (Suppl. 1), S17–S22.
Selvaraj, S., et al., 2018. Effect of citalopram on emotion processing in humans: a combined 5-HT1A [(11)C]CUMI-101 PET and functional MRI study. Neuropsychopharmacology. 43, 655–664.
Silva-Fernandes, A., et al., 2014. Chronic treatment with 17-DMAG improves balance and coordination in a new mouse model of Machado-Joseph disease. Neurotherapeutics. 11, 433–449.
Snowden, S.G., et al., 2019. Neurotransmitter imbalance in the brain and Alzheimer's disease pathology. J. Alzheimers Dis. 72, 35–43.
Stahl, S.M., 1998. Mechanism of action of serotonin selective reuptake inhibitors. Serotonin receptors and pathways mediate therapeutic effects and side effects. J. Affect. Disord. 51, 215–235.

Stothard, P., 2000. The sequence manipulation suite: JavaScript programs for analyzing and formatting protein and DNA sequences. Biotechniques. 28 (1102), 1104.
Sze, J.Y., et al., 2000. Food and metabolic signalling defects in a *Caenorhabditis elegans* serotonin-synthesis mutant. Nature. 403, 560–564.
Takei, A., et al., 2003. 'Drug holiday' effects of tandospirone in a patient with Machado-Joseph disease. Psychiatry Clin. Neurosci. 57, 607–608.
Takei, A., et al., 2004. Effects of tandospirone on "5-HT1A receptor-associated symptoms" in patients with Machado-Josephe disease: an open-label study. Clin. Neuropharmacol. 27, 9–13.
Takei, A., et al., 2005. Treatment of cerebellar ataxia with 5-HT1A agonist. Cerebellum. 4, 211–215.
Takei, A., et al., 2010. Difference in the effects of tandospirone on ataxia in various types of spinocerebellar degeneration: an open-label study. Cerebellum. 9, 567–570.
Tatum, M.C., et al., 2015. Neuronal serotonin release triggers the heat shock response in *C. elegans* in the absence of temperature increase. Curr. Biol. 25, 163–174.
Teixeira-Castro, A., et al., 2011a. Neuron-specific proteotoxicity of mutant ataxin-3 in *C. elegans*: rescue by the DAF-16 and HSF-1 pathways. Hum. Mol. Genet. 20, 2996–3009.
Teixeira-Castro, A., et al., 2011b. An Image Processing Application for Quantification of Protein Aggregates in *Caenorhabditis elegans*. Springer, Berlin Heidelberg, Berlin, Heidelberg, pp. 31–38.
Teixeira-Castro, A., et al., 2015. Serotonergic signalling suppresses ataxin 3 aggregation and neurotoxicity in animal models of Machado-Joseph disease. Brain. 138, 3221–3237.
Thampi, P., et al., 2012. The 5HT1a receptor agonist 8-Oh DPAT induces protection from lipofuscin accumulation and oxidative stress in the retinal pigment epithelium. PLoS One 7, e34468.
Trouillas, P., et al., 1997. Buspirone, a 5-hydroxytryptamine1A agonist, is active in cerebellar ataxia. Results of a double-blind drug placebo study in patients with cerebellar cortical atrophy. Arch. Neurol. 54, 749–752.
Tsalik, E.L., et al., 2003. LIM homeobox gene-dependent expression of biogenic amine receptors in restricted regions of the *C. elegans* nervous system. Dev. Biol. 263, 81–102.
Vermeiren, Y., et al., 2018. Serotonergic dysfunction in amyotrophic lateral sclerosis and Parkinson's disease: similar mechanisms, dissimilar outcomes. Front. Neurosci. 12, 185.
Vidal, B., et al., 2018. (18)F-F13640 preclinical evaluation in rodent, cat and primate as a 5-HT1A receptor agonist for PET neuroimaging. Brain Struct. Funct. 223, 2973–2988.
Vidal, B., et al., 2019. Pharmacological MRI to investigate the functional selectivity of 5-HT1A receptor biased agonists. Neuropharmacology 107867.
Vilchez, D., et al., 2012. RPN-6 determines *C. elegans* longevity under proteotoxic stress conditions. Nature. 489, 263–268.
Voisine, C., et al., 2007. Identification of potential therapeutic drugs for huntington's disease using *Caenorhabditis elegans*. PLoS One 2, e504.
Wang, Y.J., et al., 2016. Escitalopram attenuates beta-amyloid-induced tau hyperphosphorylation in primary hippocampal neurons through the 5-HT1A receptor mediated Akt/GSK-3beta pathway. Oncotarget. 7, 13328–13339.
Wang, P.S., et al., 2020a. Supratentorial and Infratentorial lesions in spinocerebellar ataxia type 3. Front. Neurol. 11, 124.
Wang, Y.J., et al., 2020b. Escitalopram alleviates Alzheimer's disease-type tau pathologies in the aged P301L tau transgenic mice. J. Alzheimers Dis. 77, 807–819.
Xie, Y., et al., 2019. The effect of selective serotonin reuptake inhibitors on cognitive function in patients with Alzheimer's disease and vascular dementia: focusing on fluoxetine with long follow-up periods. Signal Transduct Target Ther. 4, 30.
Yocca, F.D., 1990. Neurochemistry and neurophysiology of buspirone and gepirone: interactions at presynaptic and postsynaptic 5-HT1A receptors. J. Clin. Psychopharmacol. 10, 6S–12S.
van der Zande, J.J., et al., 2020. Serotonergic deficits in dementia with Lewy bodies with concomitant Alzheimer's disease pathology: an (123)I-FP-CIT SPECT study. Neuroimage Clin. 25, 102062.
Zhang, Q., et al., 2018. The mitochondrial unfolded protein response is mediated cell-non-autonomously by retromer-dependent Wnt signaling. Cell. 174 (870–883), e17.